scientific reports

Check for updates

OPEN

ZIF-67 decorated with silica nanoparticles and graphene oxide nanosheets composite modified electrode for simultaneous determination of paracetamol and diclofenac

Biuck Habibi✉, Younes Bahadori✉, Sara Pashazadeh & Ali Pashazadeh

In this work, a novel nanocomposite containing zeolitic imidazolate framework-67 decorated silica nanoparticles/graphene oxide nanosheets (ZIF-67/SiO_2NPs/GONs) was synthesized and used for the fabrication of the modified glassy carbon electrode for individual and simultaneous electrodetermination of paracetamol (PAR) and diclofenac (DIC) at trace levels. Structural and morphological characterization of the nanocomposite were carried out using suitable techniques. The modified electrode; ZIF-67/SiO_2NPs/GONs/GCE, exhibited excellent electrocatalytic activities toward the oxidation of PAR and DIC than the bare GCE, GONs/GCE, SiO_2NPs/GONs/GCE and ZIF-67/GCE. Through using differential pulse voltammetry, the individual and simultaneous determination of PAR and DIC were conducted by the ZIF-67/SiO_2NPs/GONs/GCE. Under optimal conditions, it has been observed that the calibration plots for PAR and DIC exhibit linearity within the concentration ranges of 0.5–190 (PAR) and 0.5–200 µM (DIC), with detection limits of 0.29 and 0.132 µM for PAR and DIC, respectively. The ZIF-67/SiO_2NPs/GONs/GCE shows commendable stability, reproducibility, and repeatability, and the proposed method is evaluated by individual and simultaneous determination of PAR and DIC in real samples with satisfactory results (recovery > 97%).

Keywords Paracetamol, Diclofenac, Zeolitic imidazolate framework-67, Silica nanoparticles, Graphene oxide nanosheets, Nanocomposite

Paracetamol (PAR), [acetaminophen or N-(4-hydroxyphenyl) acetamide] is one of the most widely used drugs in the world and is listed as an essential drug by the World Health Organization (WHO)[1]. The suggested PAR dosing for adults and children ≤ 12 years is 500 to 1000 mg every 4–6 h as necessary, with a maximum of 4000 mg in 24 h[2]. PAR was used as a fever medicine until the end of the nineteenth century. In 1955, due to the lake of side effects, it became available without a prescription, and its use was announced for children from one month to adults, as well as pregnant women. Medicinal forms of PAR are available in tablets, capsules and rectal suppositories[3–5]. Poisoning caused by excessive consumption of PAR and accidental ingestion by children showed that it causes severe acute and fatal liver necrosis. Consumption of 200 mg/kg in patients weighing less than 50 kg shows severe hepatotoxicity[6]. In case of a higher dose, liver transplant or death follows. As a result, there is a necessity for developing highly sensitive and selective analytical techniques for the determination of PAR in real samples. Common methods of PAR determination include spectroscopic, chromatographic, and electrochemical methods[7,8]. On the other hand, diclofenac (DIC) constitutes a pharmacological agent classified as a non-steroidal anti-inflammatory drug, employed in the managing of degenerative joint disease, sports-related injuries, postoperative pain relief, musculoskeletal injuries, and osteoarthritis[9]. Furthermore, it serves a multifaceted role as an analgesic, antipyretic, and anti-rheumatic agent[10]. Generally, DIC is offered in either 25 mg or 50 mg doses 1–4 times per day for total doses between 50 and 200 mg per 24 h[11]. The primary mechanism

Electroanalytical Chemistry Laboratory, Department of Chemistry, Faculty of Sciences, Azarbaijan Shahid Madani University, Tabriz 53714-161, Iran. ✉email: B.Habibi@Azaruniv.ac.ir; biuckhabibi.a@gmail.com; younesbahadori20@gmail.com

underlying its analgesic and anti-inflammatory properties is the inhibition of the enzyme cyclooxygenase, thereby obstructing the synthesis of prostaglandins. It is imperative to ascertain DIC concentrations at lower levels within pharmaceutical formulations and actual biological samples, attributable to its increased solubility and rapid absorption by synovial fluid[11–13]. The analytical methods for the determination of DIC that reported in the literature include spectrophotometric[14], chromatographic[15] and electrochemical methods[16]. On the other hand, the simultaneous determination of pharmaceutical compounds has gained significant attention in analytical chemistry, particularly in environmental monitoring and clinical diagnostics[17,18]. Among these compounds, PAR and DIC are widely used analgesics and anti-inflammatory medications, respectively[19]. So, their effective and simultaneous quantification is crucial due to their prevalence in medical prescriptions and potential environmental impacts[19–23]. The use of simple, inexpensive, specific and sensitive electrochemical methods for simultaneously determining of these drugs is still of interest to researchers[24]. Compared to other methods the electrochemical methods, in addition to the above benefits, have advantages such as fast response time, portability, and miniaturization[25–27]. Determination of drugs at the surfaces of unmodified electrodes has low sensitivity and selectivity, which can be increased them by modifying their surface[28]. Nanostructures such as metal nanoparticles, nanocarbons, and nanocomposites with excellent physical and chemical properties have been introduced as modifier in the fabrication of electrochemical sensors and biosensors[29–33]. Also, nowadays, in design of the electrochemical sensors and biosensors, two-dimensional materials such as layered double hydroxides, Mxenes, and metal–organic frameworks (MOFs) are increasingly being used[34–36]. MOFs are 2D materials with porous and crystalline structures composed of metal ions or clusters coordinated with organic ligands[37,38]. MOFs have been widely used in electrochemistry due to their advantages, such as high surface-to-volume area and open metal sites[39–41]. A group of MOFs, is called zeolite imidazolate frameworks (ZIFs), are a regular porous materials of metal nodes such as $Zn^{2+}$and Co^{2+} along with imidazole ligands like as 2-methylimidazole (2-MeIm)[37]. ZIFs have high porosity, high stability, and adjustable pores. Due to the structure's proper pore size and the electrocatalytic activity of metal ions, despite the lack of electrical conductivity of these materials, they are used in electrochemical sensors and biosensors[42,43]. It should be noted that, the challenge of the non-conductivity of the ZIFs is solved by integrating of them with nano carbon materials such as graphene oxide, reduced graphene oxide, carbon nanotubes, and carbon quantum dots as well as conductive nano polymers[44,45]. By combining these materials, the constructed nanocomposites will have sufficient conductivity to be used in preparing of modified electrodes as sensors and biosensors[46,47]. Graphene oxide nanosheets (GONs) exhibit significant chemical reactivity, hydrophilicity, and stability within aqueous and certain polar solvents due to presence of the abundant of oxygen-containing functional groups on their surface[31,43,46,48]. The distinctive electrochemical characteristics of GONs, along with its extensive specific surface area, facilitate the modified electrode derived from graphene oxide to substantially amplify the electronic redox signal of electrochemically active compounds, resulting in its prevalent application within the domain of sensors and biosensors[49].

Silica nanoparticles (SiO_2NPs) alone isn't suitable material for electrode modification due to its inadequate electrical conductivity and insolubility in aqueous environments, thereby make it impossible to carry out electrochemical reactions[50,51]. On the other hand, SiO_2NPs shows remarkable mechanical characteristics, encompassing substantial hardness, and longevity. Therefore, practically SiO_2NPs undergoes modification through doping and composite methodologies to enhance its electrochemical efficacy[52]. SiO_2NPs in its porous form, is exceptionally conducive to the synthesis of nanocomposite materials aimed to enhancing the functionalities of MOFs, attributable to its remarkable stability and structural versatility. SiO_2NPs serves not only as a structural substrate for MOFs nanocomposite but also as an augment material's stability through the hydrophobic interactions or covalent linkages[53–55]. The composite formation strategies involving MOFs/SiO_2NPs hybrids typically encompass an in-situ approach, wherein MOFs crystals are cultivated on the preformed SiO_2NPs, as well as the sol–gel procedure, which entails the application of a SiO_2NPs coating on the synthesized MOF crystals[56,57]. Also, the incorporating of the SiO_2NPs within GONs composites facilitates scalability and economic efficiency while preserving performance integrity, which is imperative for industrial applications. Its amalgamation into GONs composites significantly augments the mechanical stability and strength of the resultant materials. Furthermore, SiO_2NPs nanoparticles contribute to the enhancing of interlayer spacing between GONs, thereby inhibiting restacking and ensuring the retention of a substantial surface area[58–60]. As reported in the literature, the ZIF-8, SiO_2NPs, and graphene oxides nanocomposites demonstrate commendable biocompatibility, substantial surface area, effective dispersal characteristics, and rapid electron transfer capabilities, which have been utilized for both in electrochemical investigation and development of electrochemical sensors[50–61]. To date, there has no documented about the application of the ZIF-67/SiO_2NPs/GONs nanocomposite as a modifier at the GCE for the individual and simultaneous determination of PAR and DIC by electrochemical methodology. In the present investigation, the electrochemical characteristics of PAR and DIC were studied utilizing the ZIF-67/SiO_2NPs/GONs/GCE through cyclic voltammetry (CV), differential pulse voltammetry (DPV) and chronoamperometry (CA) techniques, while also assessing the influence of various experimental parameters on the electrooxidation of these compounds. Another objective of this research was the concurrent simultaneous quantification of PAR and DIC utilizing ZIF-67/SiO_2NPs/GONs/GCE through the DPV technique in real samples.

Experimental

Chemicals and apparatus

A concise elucidation of the chemicals and reagents, apparatus, and methodologies for the physicochemical characterization and electrochemical analysis are outlined in the Supporting Information.

Preparation of the SiO_2NPs/GONs

The synthesis processes of ZIFs-67[62], GONs[63] and SiO_2NPs[64] based on the literature are provided in the Supporting Information. For the preparation of the SiO_2NPs/GONs, 0.6 g of the synthesised GONs (Fig. 1, step 1) was dispersed in 50 mL of double distilled water and thoroughly mixed. Then, 0.2 g of SiO_2NPs produced from the rice husk char (RHC) via the chemical treatment and calcination (Fig. 1, step 2) was added to the mixture and stirred using a magnetic stirrer for about 60 min. After that, 5 mL of the sodium citrate solution (1%) which was boiled for about 55 min and 5 mL of sodium sulphite 0.1 M were added to the above mixture and stirred for 3 h at 100 °C. Then, the solution was cooled, filtered and washed with double distilled water and ethanol. Finally, the prepared product was dried in oven at 100 °C for about 1 h[64]. The schematic preparation steps of the SiO_2NPs/GONs were shown in the Fig. 1, step 3.

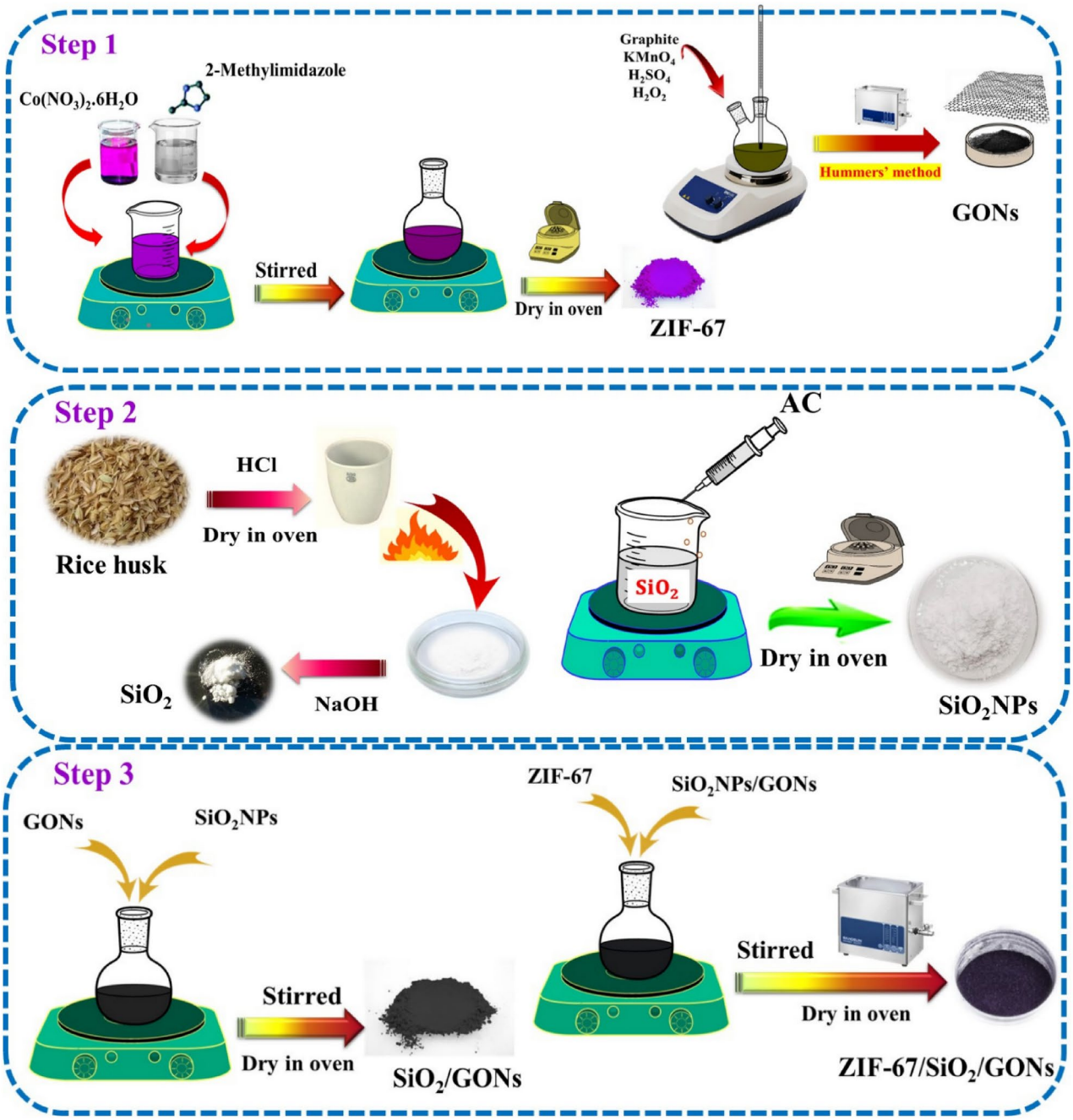

Fig. 1. Schematic synthesis steps of the ZIF-67 and GONs (step 1), SiO_2NPs (step 2), SiO_2NPs/GONs and ZIF-67/SiO_2NPs/GONs (step 3).

Preparation of the ZIF-67/SiO_2NPs/GONs

The ZIF-67/SiO_2NPs/GONs nanocomposite was prepareded by a simple precursor. Firstly, 0.06 g of ZIF-67 was dispersed in 25 mL of ethanol and ultrasonicated for about 30 min to form a homogeneous dispersion. Then, 0.02 g of SiO_2NPs/GONs was sonicated in 10 mL of ethanol for 1 h to form a dispersion. The sonicated SiO_2NPs/GONs was added into the ZIF-67 suspension and mixed by a magnetic stirring for 3 h. The mixture was dried in a vacuum oven at 70 °C for about 12 h to obtain ZIF-67/SiO_2NPs/GONs nanocomposite. The schematic preparation process of the ZIF-67/SiO_2NPs/GONs was shown in the Fig. 1 step 3.

Construction of ZIF-67/SiO_2NPs/GONs/GCE

The working approach used to modify the GCE is outlined in our previous study[65]. However, the construction process of the ZIF-67/SiO_2NPs/GONs/GCE was reported with detailed in the Supporting Information.

Results and discussion

Physicochemical characterization of the nanocomposite

The morphological and compositional characteristics of materials have significant influence on their physicochemical properties. Typical morphology of synthesized materials: GONs, SiO_2NPs/GONs, ZIF-67, and ZIF-67/SiO_2NPs/GONs are characterized by the scanning electron microscope (SEM) and presented in Fig. 2 (images of A-D). The SEM image of GONs distinctly reveals the layered architecture of GONs, featuring wrinkled sheets at the peripheries (image A). The image of SiO_2NPs/GONs clearly illustrates a consistent application of the modified SiO_2NPs, exhibiting a spherical morphology upon the surface of the GONs (image B). A magnified view of the morphology of ZIF-67 can be seen in Fig. 2 image C. From this image, it can be realized that the ZIF-67 presented perfect polyhedral shape (consistent with previous reports[66,67]). In contrast, the morphology

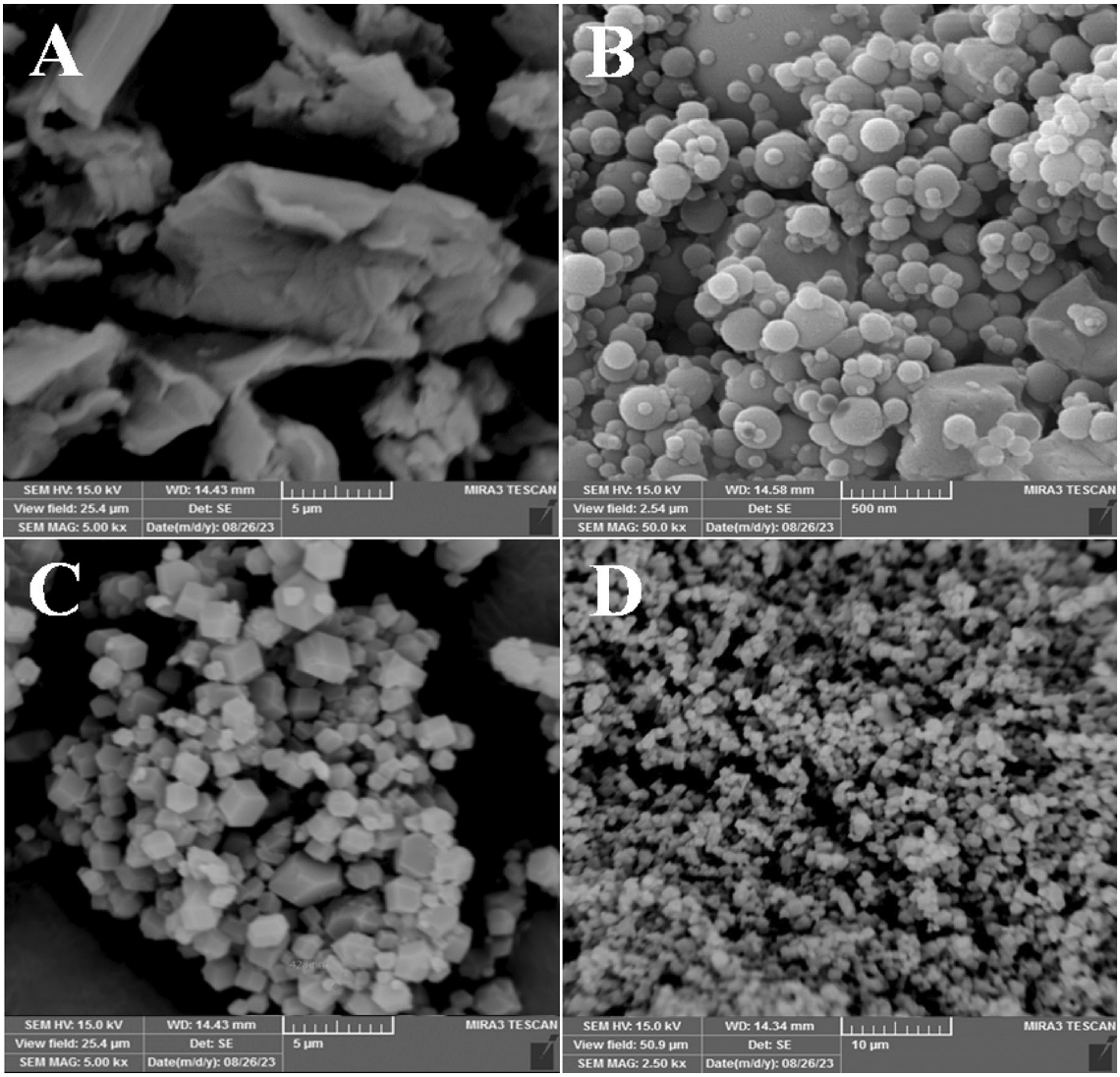

Fig. 2. SEM images of synthesized materials: (**A**) GONs, (**B**) SiO_2NPs/GONs, (**C**) ZIF-67 and (**D**) ZIF-67/SiO_2NPs/GONs.

of ZIF-67/SiO_2NPs/GONs (image D) presents a slightly uniform, wrinkled, and textured appearance. These findings imply that, despite of the presence of numerous SiO_2NPs/GONs on the surface of ZIF-67, the polyhedral morphology of the ZIF-67 preserved in perfect detail. The elemental distribution maps related to the synthesized nanocomposite, ZIF-67/SiO_2NPs/GONs, are depicted in Fig. 3 (above maps), which unequivocally demonstrates the existence of the elements Co, C, N, Si, O, and Na (alongside the corresponding weight percentages of these elements) within the sample and signifies the successful synthesis of the ZIF-67/SiO_2NPs/GONs nanocomposite devoid of any elemental impurities in its composition. Conversely, the energy-dispersive X-ray (EDX) spectrum of ZIF-67/SiO_2NPs/GONs was recoded, revealing the surface distribution of the elements of Co, C, N, Si, O, and Na, collectively. These findings are presented in Fig. 3 (lower spectrum and its inset).

X-ray diffraction (XRD) analysis was employed to examine the crystallographic configuration and phase integrity of the synthesized GONs, ZIF-67, SiO_2NPs/GONs, and ZIF-67/SiO_2NPs/GONs. In the case of the GONs sample, the observed peak at approximately $2\theta = 26.48°$ (refer to pattern b in Fig. 4) was correlated to the (002) diffraction of the organized GONs layers and exhibiting d-spacing of 3.38 Å, which is significantly greater than that of natural graphite (3.34 Å), thereby indicating the incorporation of oxygen-containing functional groups within the GONs[68]. In Fig. 4, pattern c shows the XRD of the SiO_2NPs/GONs, which reveals a substantial diminution in the diffraction intensity of the (002) plane, along with the appearance of small diffraction peaks at the $2\theta = 22°$, 45° and 53.4° in this hybrid material[69]. These findings imply that the effective integration of GONs and SiO_2NPs was achieved through electrostatic self-assembly, culminating in the formation of GONs/SiO_2NPs hybrids. In the case of ZIF-67, as illustrated in Fig. 4 (pattern d), the diffraction peaks of the synthesized ZIF-

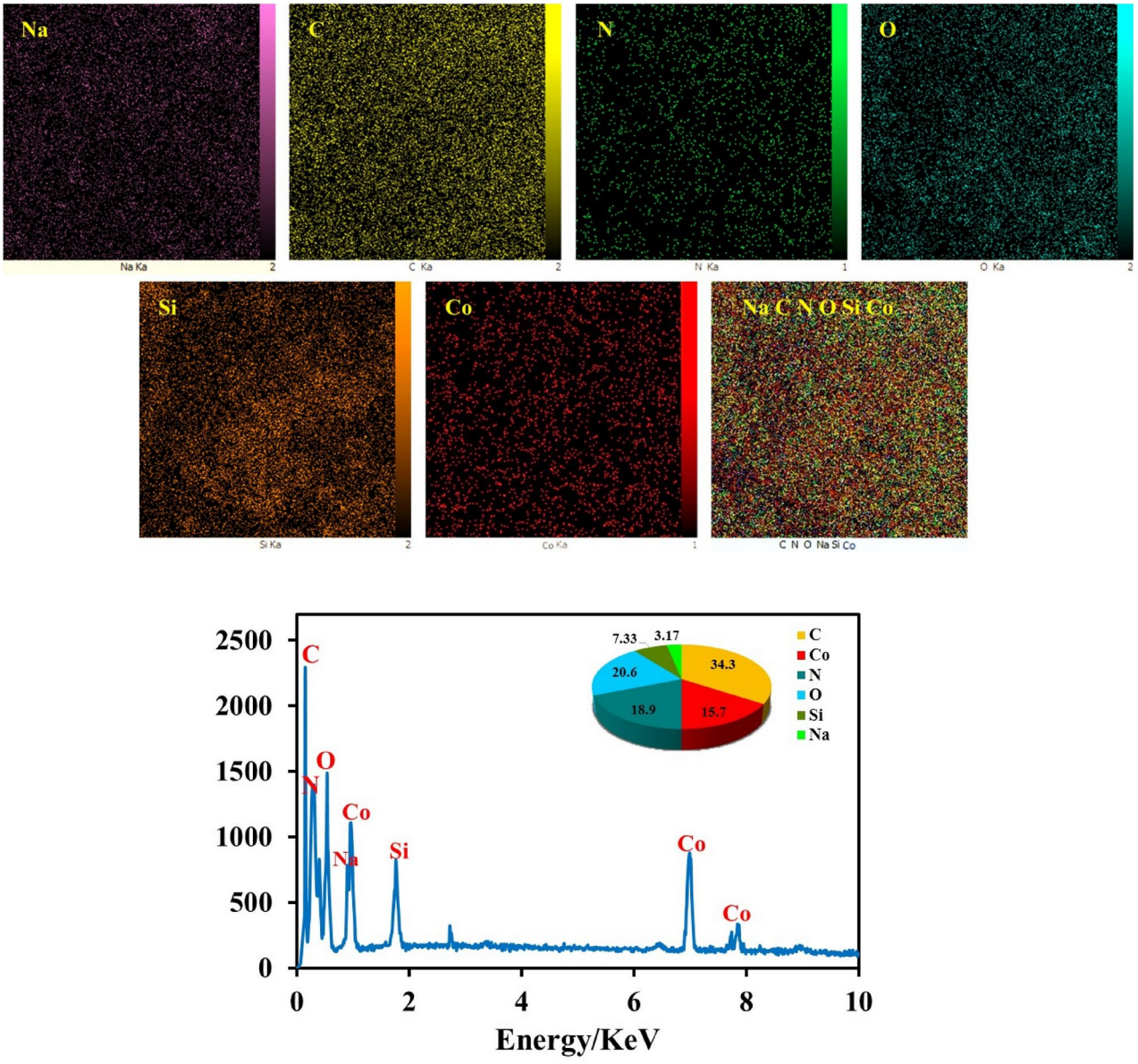

Fig. 3. Elemental mapping patterns of the ZIF-67/SiO_2NPs/GONs (above maps) and the EDX spectrum of as-prepared ZIF-67/SiO_2NPs/GONs [below (inset is percentage of atoms)].

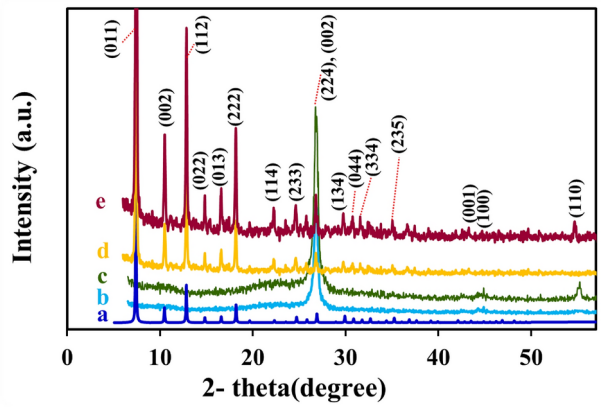

Fig. 4. XRD patterns of (**a**) simulated pattern based on single-crystal data of ZIF-67, (**b**) GONs, (**c**) SiO_2NPs/GONs, (**d**) ZIF-67 and (**e**) ZIF-67/SiO_2NPs/GONs.

67 correspond with the simulated XRD pattern for ZIF-67 (pattern a)[70,71]. The XRD pattern of ZIF-67 exhibits distinct diffraction peaks, signifying the predominance of a crystalline structure; diffraction peaks corresponding to 2θ values of 7.41°, 10.44°, 12.78°, 14.71°, 16.45°, 18.11°, 22.31°, 24.61°, 25.65°, 26.61°, 29.61°, 30.76°, 31.41°, and 32.56° can be assigned to the (011), (002), (112), (022), (013), (222), (114), (233), (224), (134), (044), (334), (244), and (235) planes, respectively[70,71]. The emergence of above peaks demonstratives the successful synthesis of ZIF-67, which was characterized by elevated crystallinity and a cubic framework (calculated lattice parameters: a = b = c = 16.9077 Å) with the Ī43m space group. The obtained results in the XRD pattern of the synthesized ZIF-67 are in good agreement with reported papers[70,71]. For the nanocomposite material, ZIF-67/SiO_2NPs/GONs, as illustrated in Fig. 4 (pattern e), all aforementioned characteristic peaks relating to ZIF-67 and SiO_2NPs/GONs are distinctly observable, thereby demonstrates the effective synthesis of ZIF-67/SiO_2NPs/GONs, characterized by a high-quality crystalline architecture.

For electrochemical characterization of the nanocomposite modified electrode along with the electrochemical properties of synthesized materials, a series of modified electrodes were fabricated namely; GONs/GCE, SiO_2NPs/GONs/GCE, ZIF-67/GCE, and ZIF-67/SiO_2NPs/GONs/GCE and tested by electrochemical methods. The cyclic voltammetric technique was implemented at the mentioned modified electrodes in the 0.1 M KCl solution containing 5 mM of $[Fe(CN)_6]^{3-/4-}$ as a redox probe. The obtained cyclic voltammograms (CVs) were illustrated in Fig. 5 A for the GONs/GCE (curve b), SiO_2NPs/GONs/GCE (curve c), ZIF-67/GCE (curve d), and ZIF-67/SiO_2NPs/GONs/GCE (curve e) which exhibit a distinct pair of redox peaks for the $[Fe(CN)_6]^{3-/4-}$, analogous to those observed at the unmodified GCE (curve a). Under identical experimental conditions, the anodic and cathodic peak currents follow a recognizable sequence of GCE < GONs/GCE < SiO_2NPs/GONs/GCE < ZIF-67/GCE < < ZIF-67/SiO_2NPs/GONs/GCE. Therefore, the ZIF-67/SiO_2NPs/GONs/GCE exhibit the highest peak currents which may originated from the favorable conductivity and high active surface area of the nanocomposite, suggesting that the ZIF-67/SiO_2NPs/GONs/GCE enhances the electron transfer rate of redux couple. Also, the electrochemical active surface area (ECSA) of the modified electrodes was determined through the cyclic voltammetric technique at various scan rates (not shown here), utilizing the Randles–Sevcik equation [Eq. (1)], as articulated in the following expression:

$$I_p = 2.69 \times 10^5 n^{3/2} A C_0 D^{1/2} \upsilon^{1/2} \quad (1)$$

The elucidation of each parameter (I_p, n, D, A, C_0, and υ) is comprehensively detailed in the extant literature that has been previously documented[72]. Through the calculations, the measured ECSA were estimated as 0.043, 0.078, 0.108, 0.125, and 0.281 cm^2 for GCE, GONs/GCE, SiO_2NPs/GONs/GCE, ZIF-67/GCE, and ZIF-67/SiO_2NPs/GONs/GCE respectively. The findings indicate that the ZIF-67/SiO_2NPs/GONs/GCE configuration has the highest ECSA and consequently the greatest number of electrochemical active sites, thereby potentially augmenting the electrochemical signals.

In addition, the conductivity properties and charge transfer of the fabricated modified electrodes were examined in 0.1 M KCl solution containing 5 mM $[Fe(CN)_6]^{3-/4-}$ using electrochemical impedance spectroscopy (EIS). As can be seen in Fig. 5B, the modified electrode coated with ZIF-67/SiO_2NPs/GONs formed a semicircle with a smaller diameter than the bare and other modified GCE. Randles equivalent circuit electrode (Rct) values for the bare GCE being approximately 385 Ω. While, following the modification, the R_{ct} decreased to the 293.5 Ω for the GONs/GCE, 265 Ω for SiO_2NPs/GONs/GCE, 220 Ω for the ZIF-67/GCE and finally 175 Ω for the ZIF-67/SiO_2NPs/GONs/GCE, thereby indicating the enhanced conductivity of the final nanocomposite modified electrode; ZIF-67/SiO_2NPs/GONs/GCE. This enhancement in the conductivity properties can be ascribed to the increased charge transfer kinetics associated with ZIF-67/SiO_2NPs/GONs/GCE. On the other hand, these values are interpreted as a simple electron exchange between the constructed modified electrodes with $[Fe(CN)_6]^{3-/4-}$ and the strong conductivity of the main developed nanocomposite; ZIF-67/SiO_2NPs/GONs[37,41,43,65].

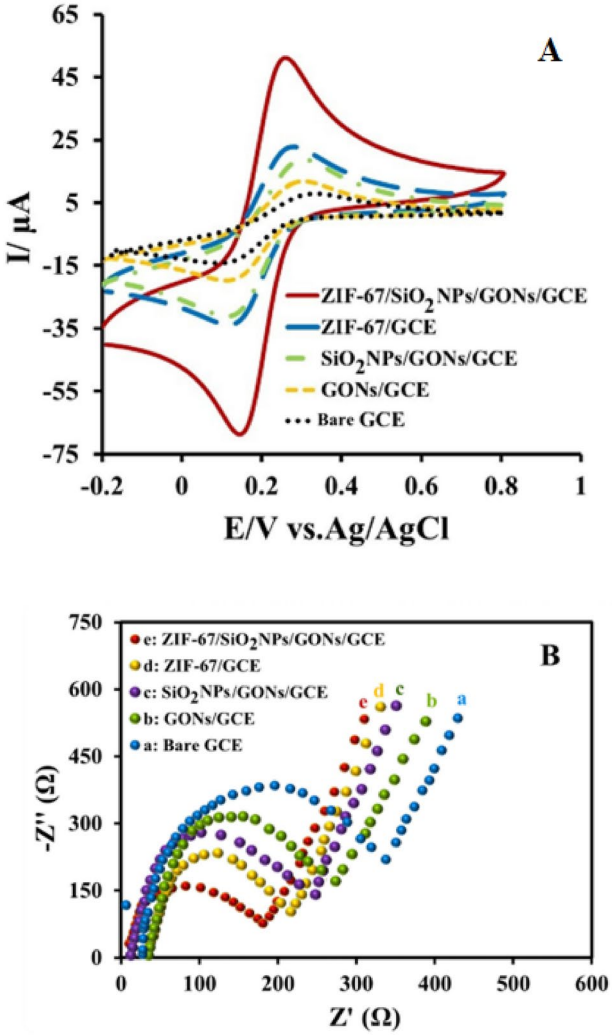

Fig. 5. (**A**) CVs of the bare GCE, GONs/GCE, SiO_2NPs/GONs/GCE, ZIF-67/GCE, ZIF-67/SiO_2NPs/ GONs/GCE in 0.1 M KCl solution containing 5 mM $[Fe(CN)_6]^{3-/4-}$ scan rate of 100 mV/s. (**B**) EIS spectra of the same electrodes in the same solution.

Electrocatalysis activity of the ZIF-67/SiO_2NPs/GONs/GCE

The electrocatalysis characteristics and comparative evaluation of the electrocatalytic activity of the ZIF-67/SiO_2NPs/GONs/GCE are investigated utilizing the cyclic voltammetric method. The CV response of the ZIF-67/SiO_2NPs/GONs/GCE toward the electrooxidation of PAR (0.2 mM) within the potential range of -0.15 to 0.80 V relative to Ag/AgCl in a phosphate buffer solution (PBS) (0.1 M, pH = 7.0) at a scan rate of 100 mV/s is documented and illustrated along with the responses of unmodified GCE, GONs/GCE, SiO_2NPs/GONs/GCE and ZIF-67/GCE in Fig. 6A. As depicted in Fig. 6A (curve a), the unmodified GCE demonstrates negligible electrochemical activity concerning the oxidation of PAR. Also, the GONs/GCE (curve b) and SiO_2NPs/GONs/GCE (curve c) show the anodic currents slightly more than the unmodified GCE. In fact, the GONs/GCE and SiO_2NPs/GONs/GCE don't have any specific electrocatalysis activity toward the oxidation of PAR in the present conditions. In contrast, the CV curves for the ZIF-67/GCE and ZIF-67/SiO_2NPs/GONs/GCE exhibit distinct oxidation peaks, with peak currents as 7.41 μA for the ZIF-67/GCE (curve d) and 18.31 μA for the ZIF-67/SiO_2NPs/GONs/GCE (curve e). On the other hand, at the ZIF-67/SiO_2NPs/GONs/GCE, the oxidation peak of PAR appeared at + 435 mV (in comparison to + 595 mV at the unmodified GCE). Furthermore, as evidenced in Fig. 6A (curve e), the ZIF-67/SiO_2NPs/GONs/GCE manifests a clearly defined and significant peak for the oxidation of PAR, exhibiting the highest current output compared to all previously mentioned incrementally modified GCEs. The findings suggest that the oxidation process of PAR on the surface of the GCE is markedly enhanced due to the incorporation of ZIF-67/SiO_2NPs/GONs nanocomposite, which not only preserves the conductivity of GONs but also augments its electrocatalytic efficacy through an increased active surface area. Additionally, as elucidated, this phenomenon characterized by the superior electrocatalytic performance of the ZIF-67/SiO_2NPs/GONs/GCE toward PAR oxidation may be attributed to the elevated specific surface area of ZIF-67 and GONs, along with the synergistic interactions among the GONs, SiO_2NPs, and ZIF-67, which facilitate exceptional electron transfer capabilities and enhanced electrocatalytic activity. In fact, the significant

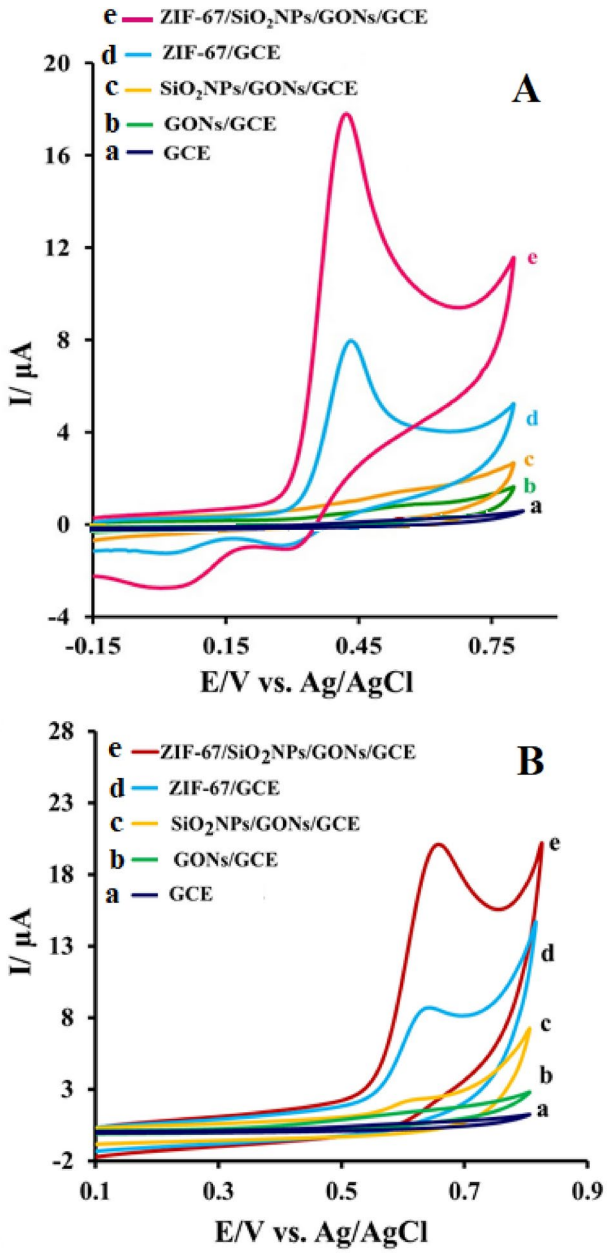

Fig. 6. (**A**) CVs of the PAR and (**B**) CVs of the DIC at the GCE (a), GONs/GCE (b), SiO_2NPsNPs/GONs/GCE (c), ZIF-67/GCE(d) and ZIF-67/SiO_2NPsNPs/GONs/GCE (e), respectively. Cyclic voltammetric conditions: scan rate of 100 mV/s for 0.2 mM of PAR and 0.2 mM of DIC in 0.1 M PBS (pH = 7.0).

enhancement in the current response of PAR indicates that the ZIF-67/SiO_2NPs/GONs/GCE accelerates the rate of electron transfer, thus functioning as a catalyst for the electrochemical reaction. Ultimately, as observed in Fig. 6A, the absence of a sharp reduction peak and unequivalent to anodic peak for PAR during the reverse scan suggests that the oxidation of PAR at the ZIF-67/SiO_2NPs/GONs/GCE is a semi-irreversible process, as inferred from our experimental outcomes and scientific observations[4,21,23,73,74].

The electrochemical response of the ZIF-67/SiO_2NPs/GONs/GCE was similarly explored in the presence of DIC. For this purpose, the CV plot of the DIC (0.2 mM) was recorded at the bare GCE, GONs/GCE, SiO_2NPs/GONs/GCE, ZIF-67/GCE and ZIF-67/SiO_2NPs/GONs/GCE in the potential window of 0.10 to 0.80 V vs Ag/AgCl in PBS (pH = 7.0) with a scan rate of 100 mV/s (Fig. 6B). As shown in Fig. 6B, each CV curve has oxidation peak with peak current as 0.82 µA (unmodified GCE, curve a), 1.63 µA (GONs/GCE, curve b), 2.31 µA (SiO_2NPs/GONs/GCE, curve c), 8.61 µA (ZIF-67/GCE, curve d), and 20.13 µA (ZIF-67/SiO_2NPs/GONs/GCE, curve e). on the other hand, at the ZIF-67/SiO_2NPs/GONs/GCE, the oxidation peak of DIC appeared at + 644 mV (in comparison to + 689 mV at the bare GCE)[13,16,17,21–23]. Notably, the ZIF-67/SiO_2NPs/GONs/GCE shows a remarkable transition in the anodic peak potential, toward lower potential, from + 595 to + 435 mV for PAR and from + 689 to + 644 mV for DIC together with a 20–25 folds enhancement in anodic peak currents

of PAR and DIC when compared to the bare GCE. These results, especially the sufficient potential difference between the oxidation of these two compounds, suggest an efficient interfacial charge transfer process occurring at the developed modified electrode. Consequently, the ZIF-67/SiO_2NPs/GONs/GCE was used as a sensor for the individual and simultaneous determination of the PAR and DIC.

Effect of the type of supporting electrolyte and pH on the electrocatalytic activity

One of the essential factors that could affect the electrocatalytic activity of the modified electrodes is the type of supporting electrolyte, which can alters the electron interaction between the electrode and analytes. The electrochemical responses of PAR and DIC at the ZIF-67/SiO_2NPs/GONs/GCE were studied in different buffer solutions such as PBS, Britton-Robinson buffer and acetate buffer solution. The results showed that the anodic peak currents of PAR and DIC in PBS are more than others supporting electrolyte and PBS has an effective role in the voltammetric responses (data not shown here). Therefor the PBS was selected as the supporting electrolyte for all experiments.

Considering the results of others' work, pH of PBS will play a considerable effect on the oxidation responses of PAR and DIC at the ZIF-67/SiO_2NPs/GONs/GCE[75–79]. Therefore, the effect of pH was investigated on the electrooxidation of PAR at the modified electrode utilizing cyclic voltammetric technique across several distinct pH levels. Figure 7 shows the obtained CVs (A), oxidation peak current, and peak potential (B) of PAR (0.2 mM) in 0.1 M PBS with different pH in the ranges of 2.0 to 9.0. As can be seen, the CV grams of the PAR changed with the pH of PBS. On the other hand, the peak current values increase at pH between 2.0 and 7.0 due to the participation of protons. Peak current values higher than pH = 7.0 show a decrease in current due to the weak oxidation reaction of PAR, which is kinetically less favorable. The optimal pH of the PBS was chosen based on the maximal peak current in pH = 7.0. As observed in Fig. 7B, the peak potential of PAR oxidation changes to a high negative value with increasing of pH. There was a linear relationship between peak potential of PAR oxidation and pH, and the regression equation is as follows:

$$E_p\,(V) = 0.7071 - 0.0461\ pH \quad \left(R^2 = 0.9929\right) \tag{2}$$

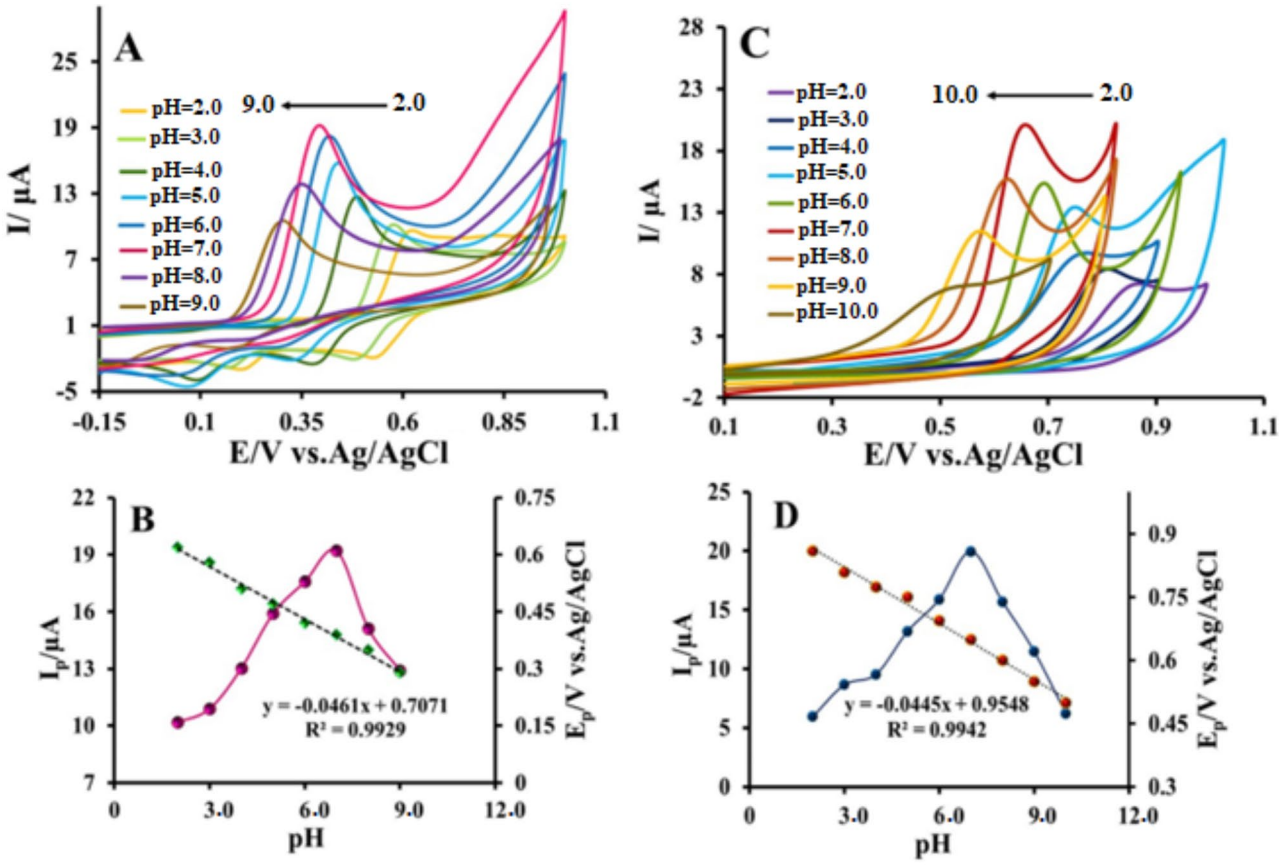

Fig. 7. (**A**) CVs of the ZIF-67/SiO_2NPs/GONs/GCE in 0.1 M PBS with different pH from 2 to 9 in the presence of 0.2 mM PAR at a scan rate of 100 mV/s, (**B**) the effect of pH value on the I_p and E_p of PAR oxidation, (**C**) CVs of the ZIF-67/SiO_2NPs/GONs/GCE in 0.1 M PBS with different pH values from 2 to 10 in the presence of 0.2 mM DIC at a scan rate of 100 mV/s and (**D**) effect of pH value on the I_p and E_p of the DIC oxidation.

The slope of E_p against the pH graph, 0.0461 (V/pH), exhibits a remarkable proximity to the theoretical value of 0.0591 V/pH (Nernst slope), thereby substantiating the participation of an equivalent quantity of protons and electrons in the electrochemical reaction associated with the redox process of PAR. Furthermore, Fig. 8 delineates a probable electrochemical reaction mechanism for PAR, wherein the PAR molecule facilitates the transfer of $2e^-$ and $2H^+$ to yield the corresponding oxidized species[75]. These findings are congruent with previously documented researches[76–79]. Also, the effect of pH on the electrooxidation of DIC at the ZIF-67/SiO_2NPs/GONs/GCE was investigated. Similar to the electrooxidation of PAR at this modified electrode, the resulting CVs (Fig. 7C) were proportionally changed with pH, and DIC oxidation behavior depend on the pH of the PBS. The correlation between the peak current and peak potential in oxidation of DIC and the pH (in the range of 2.0 to 10.0) are explored by a linear relationship (Fig. 7D), represented by the regression equation: $E_p(V) = 0.9548 - 0.0445$ pH ($R^2 = 0.994$)[80,81]. The slope of the peak potential versus pH value was obtained to be 0.0445 V/pH which is close to the Nernstian value of 0.0591 V/pH. The slope of 0.0445 V/pH indicates that the equal number of electrons and protons are participate in the redux process which is well in accordance with the earlier reports[80,81]. The mechanism of the electrooxidation of DIC is also shown in Fig. 8[81].

Effect of potential scan rate on the electrochemical behaviors of the PAR and DIC

In order to obtain useful electrochemical information from the oxidation of PAR and DIC at the ZIF-67/SiO_2NPs/GONs/GCE, it is imperative to understand the effect of the potential scan rate on their electrochemical behaviors. This investigation for PAR (0.2 mM) was performed utilizing the cyclic voltammetric technique, while systematically varying the potential scan rate from 5 to 120 mV/s in PBS (0.1 M, pH = 7.0). Figure 9 A shows the CVs of the ZIF-67/SiO_2NPs/GONs/GCE in different potential scan rate. As can be seen, the CV currents increase as the scanning rate changes to high values. The depicted data in Fig. 9 B indicates that the anodic and cathodic peak currents exhibited a linear increase with respect to the square root of the scan rate ($\upsilon^{0.5}$). The resulting plot, anodic peak current (I_{pa}) as function of $\upsilon^{0.5}$ for PAR at the ZIF-67/SiO_2NPs/GONs/GCE, is characterized by an exemplary linearity represented by the equation; I_{pa} (μA) = 4.3666 + 2.072 $\upsilon^{0.5}$, with a correlation coefficient (R^2) of 0.9904. This observation implies that the electrooxidation mechanism of PAR at the ZIF-67/SiO_2NPs/GONs/GCE is governed by a diffusion-controlled process. Furthermore, a direct correlation was established between the logarithm of the anodic and cathodic peak currents (Log I_{pa} and Log I_{pc}) and the logarithm of the scan rate (Log υ), with a slope of 0.6052 for the anodic part (Fig. 9C). This slope is in close proximity to the theoretically anticipated value of 0.5 for processes that are diffusion-controlled[65]. Also, as mentioned in the literature, one of the common ways to predict the electrode process mechanism using cyclic voltammetry data is the examine the dependence of the current function (normalized current relative to the square root of the potential scan rate ($I_{pa}.\upsilon^{0.5}$) to the square root potential scan rate (Fig. 9D). The increase of the current function proportional to the increase of the scan rate and reaching its to constant values indicates the existence of the electron transfer

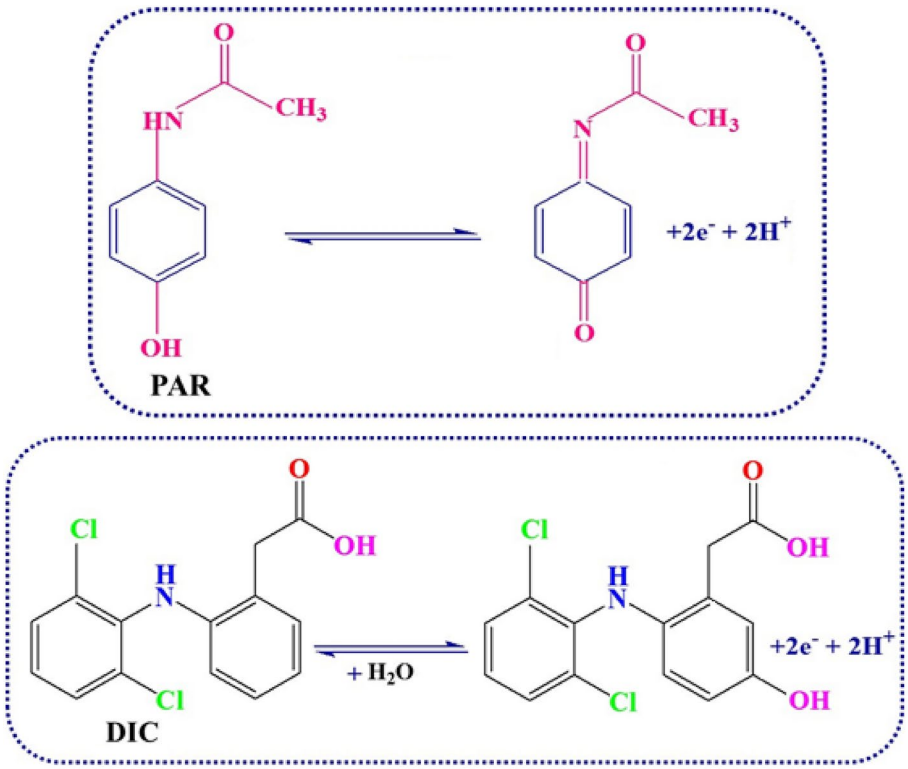

Fig. 8. The electrochemical oxidation mechanism of PAR and DIC at the ZIF-67/SiO_2NPs/ GONs/GCE in natural solution.

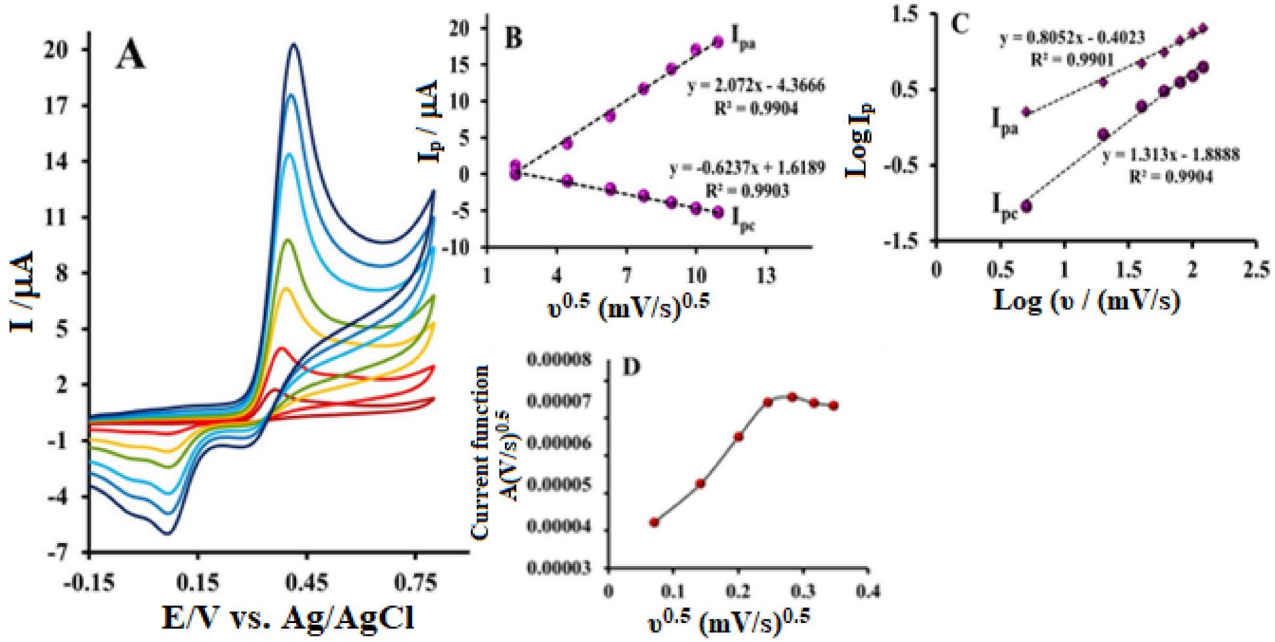

Fig. 9. (**A**) CVs obtained at the ZIF-67/SiO_2NPs/GONs/GCE in 0.1 M PBS (pH = 7.0) containing 0.2 mM PAR solution at different scan rates (5–120 mV/s), the plot of (**B**) anodic and cathodic currents (I_{pa} and I_{pc}) vs. $\upsilon^{0.5}$, (**C**) Log anodic and cathodic currents (I_{pa} and I_{pc}) vs. Log υ and (**D**) variation of the catalytic anodic current multiple with the square root of scan rate (current function)(I . $\upsilon^{0.5}$) vs. $\upsilon^{0.5}$ (square root of scan rate) (V) for 0.2 mM PAR in 0.1 M PBS solution.

following chemical reaction (EC) mechanism[82–84]. The low cathodic current in the reverse scan is an indication of this mechanism. Additionally, a linear relationship was identified between the anodic peak potential (E_{pa}) and the logarithm of the scan rate (Log υ) within the range of 5–120 mV/s (not shown here). Consequently, as the scan rate was incrementally increased, a corresponding shift in the potential toward more positive values was observed, thereby verifying the presence of kinetic limitations within the electrochemical reaction. To further elucidate details regarding the rate-determining step, the Tafel plot was constructed from the recorded CVs at low scan rate for the ZIF-67/SiO_2NPs/GONs/GCE in the presence of 0.2 mM PAR (not depicted here). The Tafel slope was calculated as 73 mV/decade, indicating that the rate-limiting step encompasses a two-electron transfer process (utilizing the Tafel equation: slope = (1 − α)nF/2.303RT). Moreover, the electron transfer coefficient for PAR was determined as 0.54. Furthermore, in accordance with Laviron's theory regarding to irreversible electrode processes, the catalytic rate constant (k_s) was derived from the E_{pa}-Log υ plot (not shown) and the corresponding equation (Eq. 3), where n, F, R, T, and other symbols are assigned their conventional meanings[72].

$$E_{pa} = E^0 + \left(\frac{2.303RT}{\alpha nF}\right) log\left(\frac{RTK_s}{\alpha nF}\right) + \left(\frac{2.303RT}{\alpha nF}\right) \log\upsilon \tag{3}$$

Employing the Laviron equation, the calculated value for k_s was determined as 1.63 s^{-1}.

In the context of oxidation of DIC, according to the Laviron equation, the observed linear positive displacement of E_{pa} with increasing of log υ serves as an indicator of the irreversible reaction mechanism (within the range of 5–120 mV/s). The solp of E_{pa} in relation to log υ indicates that the DIC oxidation is characterized as a two-electron transfer mechanism (Fig. 8).

Chronoamperometric study

To assess and estimate of the diffusion coefficients (D, cm^2/s) of PAR and DIC, chronoamperometric analyses were firstly conducted concerning the oxidation of PAR at the interface of ZIF-67/SiO_2NPs/GONs/GCE in 0.1 M PBS (pH = 7.0) by applying the potential of 0.421 V vs Ag/AgCl. The resultant chronoamperograms at various concentrations of PAR are presented in Fig. 10 A. Subsequently, the experimental graphs depicting the current (I) as a function of $t^{-1/2}$ were established and shown in inset (I) of Fig. 10 A. It is evident that the plots of anodic current in relation to the inverse square root of time (I α $t^{-1/2}$) across different PAR concentrations exhibit a linear relationship. This observation verifies that a diffusion mechanism governs the transient anodic current associated with the electrooxidation of PAR. The diffusion coefficient of PAR in chronoamperometric study was obtained via Cottrell equation[85].

$$\mathrm{I} = \mathrm{nFAD}^{1/2}C^*(\pi t)^{-1/2} \tag{4}$$

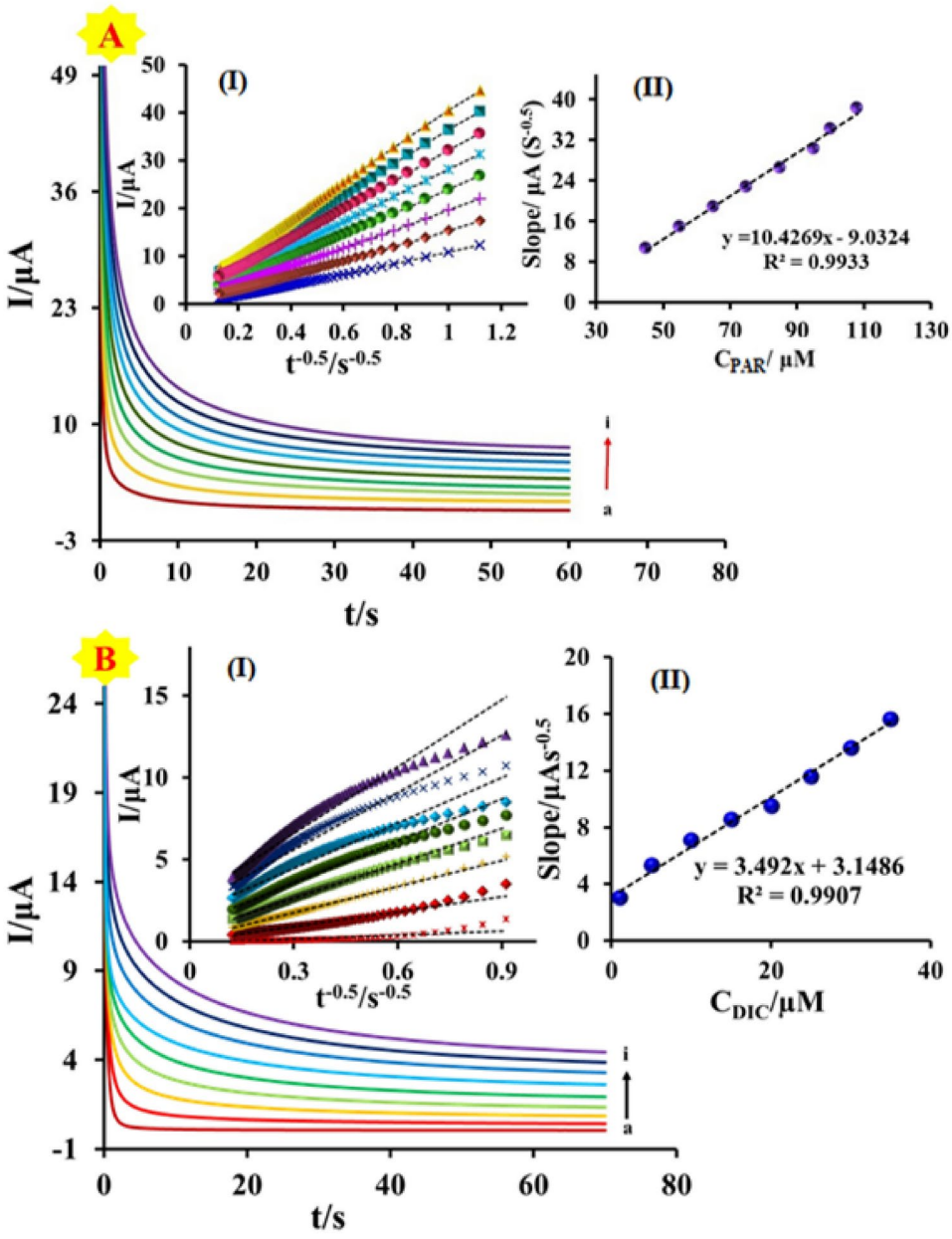

Fig. 10. (**A**) Chronoamperograms obtained in 0.1 M PBS (pH = 7.0) in the absence (a) and presence of PAR (b-i: 45, 55, 65, 75, 85, 95, 100 and 108 μM) at ZIF-67/SiO_2NPs/GONs/GCE. Insets: plot of I vs. $t^{-1/2}$ obtained from chronoamperograms (I) and plot of the slope of the straight lines against PAR concentrations (II). (**B**) Chronoamperograms obtained in 0.1 M PBS (pH = 7.0) in the absence (a) and presence of DIC (b-i:1, 5, 10, 15, 20, 25, 30 and 35 μM) at ZIF-67/SiO_2NPs/GONs/GCE. Insets: plot of I vs. $t^{-1/2}$ obtained from chronoamperograms (I) and plot of the slope of the straight lines against DIC concentrations (II).

where D is the diffusion coefficient (cm^2/s), A is electrode surface area (cm^2) and C^* is the concentration (mol/cm^3) of the analyte. The graph of I versus $t^{-1/2}$ is linear under diffusion control with a slope corresponding with diffusion coefficient. The slope of the resulting lines in Fig. 10 A was plotted against PAR concentration and from its slope the diffusion coefficient can be calculated. Inset (II) in Fig. 10 A shows the plot of slops vs concentration of PAR. The value of diffusion coefficient for PAR was calculated as 1.56×10^{-6} cm^2/s. The diffusion coefficient of DIC was also determined utilizing the chronoamperometric technique. The chronoamperograms representing DIC oxidation at different concentrations in 0.1 M PBS pH = 7.0 at the surface of the ZIF-67/SiO_2NPs/GONs/GCE are depicted in Fig. 10 B. In this section, the experimental graphs depicting the current (I) as a function of $t^{-1/2}$ was drawn [inset (I)], followed by the construction of the slopes graph corresponding to the slope of the resulting lines against DIC concentrations [inset (II)]. Based on the slope of the final graph [inset (II)] and employing Eq. (4), the diffusion coefficient of DIC was estimated as 2.83×10^{-6} cm^2/s.

Individual determination of PAR and DIC at the ZIF-67/SiO_2NPs/GONs/GCE

The individual determination of PAR at the ZIF-67/SiO_2NPs/GONs/GCE under optimal conditions was determined by differential pulse voltammetry (DPV) technique. Different concentrations of PAR in PBS (0.1 M, pH = 7.0) were analyzed at the ZIF-67/SiO_2NPs/GONs/GCE (Fig. 11A). As can be seen, the anodic peak current of PAR increased linearly with increasing its concentration. The anodic peak current versus concentration of PAR was linear in the ranges of 0.5 to 190 µM (inset of Fig. 11A). The limit of detection (LOD) of this method was calculated as 0.29 ± 0.2 µM (S/N = 3). The sensitivity of the modified electrode toward the oxidation of PAR was determined from the calibration curve as 0.129 µA/µM. The high anodic peak current, low LOD and good sensitivity indicate that the ZIF-67/SiO_2NPs/GONs/GCE can be used as sensor for detection of PAR. The performance of proposed sensor, ZIF-67/SiO_2NPs/GONs/GCE, for determination of PAR is compared with other modified electrodes in the literature and listed in Table 1. The undeniable advantages of the present sensor in Table 1, together with other benefits such as simple fabrication method, low-cost equipment and less operating time compared to other sensors, indicate that ZIF-67/SiO_2NPs/GONs/GCE will be a practical electrochemical sensor for PAR detection.

In the case of DIC, the anodic peak current exhibited a linear relationship with its concentration within the specified ranges of 0.5–200 µM, which were recorded by DPV (Fig. 11 B) and plotted on a graph (inset of Fig. 11 B). The respective linear regression equation was delineated as I_p (µA) = 0.209 C_{DIC} (µM) + 1.5369 (R^2 = 0.9957). The LOD was determined as132 nM for individual DIC determination. The sensitivity of the modified electrode toward the detection of DIC was determined as 0.1233 µA/µM. The performances of proposed modified electrode, ZIF-67/SiO_2NPs/GONs/GCE, in electrodetermination of DIC is compared with other modified electrodes in the literature and listed in Table 2. As can be seen, the linear dynamic range and LOD of the proposed sensor for determining DIC are comparable/superior to some previously published papers.

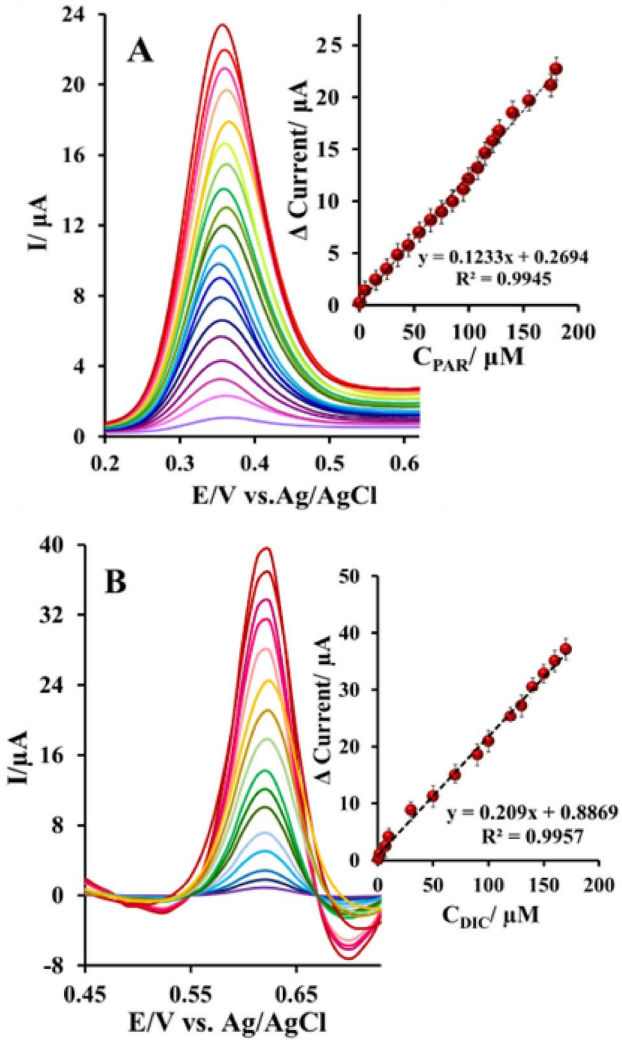

Fig. 11. DPVs of the ZIF-67/SiO_2NPs/GONs/GCE in various concentration PAR (0.5–190 µM) (**A**) and different concentrations DIC in the range 0.5–200 µM (**B**). Insets are the relationship of delta current responses to PAR and DIC concentrations.

Modified electrode	Linear range (μM)	Detection limit (μM)	References
GO-XDA-Mn_2O_3[1]	1–1000	0.056	86
Co_3O_4NPs@HCCC-rGO[2]	0.1–11	0.0646	87
Co–La oxides/CNF[3]	5–1600	0.25	88
H-C/N@TiO_2[4]	0.3–50	0.05	89
$ZnFe_2O_4$/SPE[5]	0.5–500	0.29	90
fCNT/PMG/CE[6]	25–200	4.3	91
PMMCNTPE[7]	2–50	0.38	92
MWCNTs–COOH/GCE[8]	0.5–50	0.2	93
ER-GO/GCE[9]	1–10	0.025	94
exf-NGr/GCE[10]	0.1–100	0.00303	95
GNPs-Naf/SPE[11]	0.25–30	0.25	96
P-NC/GCE[12]	3–110	0.5	97
PS-PNIPAm-PS-MWCNTs-GQDs[13]	1–7,7–100	0.066	98
SWCNT–GNS/GCE[14]	0.05–64.5	0.038	99
MWCNT/GO/Poly(Thr)/GCE[15]	5–200	0.16	100
Cu-MOF/ERGO/GCE[16]	0.2–160	0.016	101
ZnNC-rGO(800)[17]	0.5–70	0.077	102
RGO/Chit/CB/GCE[18]	2.8–190	0.053	103
$Co(OH)_3$/GCE[19]	50–550	1.83	104
Pd-Schiff base/GCE[20]	1–50	0.067	105
CeO_2-Cu_2O/Pt/CPE[21]	0.4–32	0.05	106
Zn-MOF/GCE[22]	1–5, 5–80	0.104	107
$[Co(HDM)_2(H_2O)_2]$/GCE[23]	5–20	1.666	108
ZIF-67/SiO_2NPs/GONs/GCE	0.5–190	0.29	This work

Table 1. Comparison of analytical characteristics of the ZIF-67/SiO_2NPs/GONs/GCE for the determination of PAR with other modified electrodes. 1 Graphene oxide-1,4-xylenediamine-manganese oxide. 2 Cobalt oxide nanoparticles@hollow carbon chamfer cube-reduced graphene oxide. 3 Cobalt-lanthanum oxides/carbon nano fiber. 4 N-doped carbon@TiO_2 double-shelled hollow sphere. 5 Zinc ferrite nanoparticles/screen-printed carbon electrode. 6 Functionalized carbon nanotubes/poly(methylene green)/graphite composite electrode. 7 Poly (methyl orange) modified carbon nanotube paste electrode. 8 Multi-wall carboxylated carbon nanotubes/glassy carbon electrode. 9 Electrochemically reduced graphene oxide/Nafion glassy carbon electrode. 10 Nitrogen-doped graphene/glassy carbon electrode. 11 Graphene nanoplatelets-Nafion/screen-printed electrode. 12 Nitrogen-rich porous carbon/glassy carbon electrode. 13 Poly(styrene-*b*-(*N*-isopropylacrylamide)-*b*-styrene)-carboxylated multi-walled carbon nanotubes- amino-functionalized graphene quantum dots. 14 Single-walled carbon nanotube-graphene nanosheets/glassy carbon electrode. 15 Poly l-threonine/graphene oxide/multi-walled carbon nanotube/glassy carbon electrode. 16 Copper metal organic framework/electroreduction graphene oxide/glassy carbon electrode. 17 Zeolitic imidazolate frameworks and graphene oxide derived ^3D–^2D Zn/N-doped carbon. 18 Reduced graphene oxide/carbon black/chitosan/glassy carbon electrode. 19 Cobalt hydroxide nanoparticles/glassy carbon electrode. 20 Self-assembly Pd (II)-schiff base/glassy carbon electrode. 21 Cerim oxide-copper oxide/palatium/carbon paste electrode. 22 Zn-based metal–organic framework/glassy carbon electrode. 23 Cobalt azo dye ligand complex/glassy carbon electrode.

Simultaneous determination of PAR and DIC at the ZIF-67/SiO_2NPs/GONs/GCE

In this section, the simultaneous determination of PAR and DIC was performed. To assess the independence of each compound's signal from the other compound; PAR and DIC, three distinct experimental setups were conducted in the 0.1 M PBS (pH = 7.0). In the first two experimental procedures, the concentration of one compound was systematically altered while the concentration of the other compound remained constant, and in the final study the concentration of both compounds was changing incrementally. In fact, the anodic peak current of DIC should be increased with increasing the concentration of DIC while the concentration and anodic peak current of PAR are constant and vice versa. Figure 12 A illustrates the DPVs of the mixture where in the concentration of DIC is increased form 20–160 μM (inset: calibration curve for DIC in the range of 20–160 μM) while the concentration of PAR is held constant (75 μM). In the second experiment, the concentration of DIC was fixed at the 50 μM and concentration of PAR was increased from 20 to 150 μM (Fig. 12 B) (inset: calibration curve for PAR in the range of 20–150 μM). Finally, the efficacy of the ZIF-67/SiO_2NPs/GONs/GCE for the simultaneous quantification of PAR and DIC was validated by varying the concentrations of both compounds. Figure 13 shows the DPVs revealed two distinctly defined anodic peaks at potentials of 375 mV and 640 mV for PAR and DIC with increasing in the anodic peak currents by increasing their concentrations. This further corroborated that the oxidation of PAR at the modified electrode occurs entirely independently and is

Modified electrode	Linear range (μM)	Detection limit (μM)	References
Au-PtNPs/f-MWCNTs/AuE[1]	0.5–1000	0.3	109
MWCNT/TiO_2/CPE[2]	1.1–5000	0.33	110
MWCNTs-IL-CPE[3]	0.5–300	0.2	111
Tyrosine-CPE[4]	10–140	3.28	112
ZnO nanoflowers/ SPE[5]	0.01–40	0.1	113
Oxidizedg-C_3N_4/CuAl-LDH/GCE[6]	0.5–60	0.38	114
VFMCNTCPE[7]	5–600	2.0	115
f-MWCNTs/GCE[8]	2–15	0.1	116
MI PANI/rGO/CPE[9]	15.71–251.50	2.88	117
NHMNE[10]	196–2650	31.7	118
GCE/DBA/DCF[11]	0–1000	0.27	119
BDD[12]	5–50	0.14	120
GE[13]	2.56–9.5	0.76	121
ISE[14]	10–10,000	4	122
BFE[15]	6–50	4.3	123
CNTPE[16]	2–100	0.8	124
Cu-Al LDH/CFYM/GPGE[17]	1.99–23.44	1.91	125
ZIF-67/SiO_2NPs/GONs/GCE	0.5–200	0.132	This work

Table 2. Comparison of analytical characteristics of ZIF-67/SiO_2NPs/GONs/GCE for the determination of DIC with other modified electrodes. 1 Au-Pt bimetallic nanoparticles/multi-walled carbon nanotubes/gold electrode. 2 Titanium oxide Nanoparticles- multi-walled carbon nanotubes /carbon paste electrode. 3 Ionic liquid-multi-walled carbon nanotubes /carbon paste electrode. 4 Tyrosine-carbon paste electrode. 5 Zinc oxide nanoflowers-screen-printed electrode. 6 oxidized graphitic carbon nitride-copper–aluminium layered double hydroxide/glassy carbon electrode. 7 vinylferrocene/multiwall carbon nanotubes/carbon paste electrode. 8 functionalized multi-walled carbon nanotubes/glassy carbon electrode. 9 Imprinted polymer-polyaniline-reduced graphene oxide/carbon paste electrode. 10 Nickel hydroxide-nickel electrode. 11 Sodium diclofenac/amino-functionalized diclofenac binding aptamer/glassy carbon electrode. 12 Boron-Doped Diamond Electrode. 13 Graphite electrode. 14 Ion-selective electrode. 15 Bismuth film electrode. 16 Carbon nanotubes paste electrode. 17 Copper–Aluminium layered double hydroxide/chicken feet yellow membrane graphenized pencil graphite electrode.

devoid of any influence from DIC and vice versa. Inset (A) in Fig. 13 shows the calibration plot of ΔIp vs. PAR concentrations and inset (B) shows the calibration plot of ΔIp vs. DIC concentrations.

Interferences effects on the responses of the ZIF-67/SiO_2NPs/GONs/GCE

In practical applications of a sensor, a major concern is the potential impact of interfering substances that may be present in real samples and alter the signal of sensor. The study was examined how various compounds commonly found alongside PAR and DIC in pharmaceuticals could affect the determination of PAR and DIC at the ZIF-67/SiO_2NPs/GONs/GCE under optimal conditions. The tolerance limit was established as the concentration ratio of interference/PAR and DIC that resulted a less than ± 5% relative error. The obtained results demonstrated that an excess of K^+ and Na^+ (group I) up to 200-fold and Ca^{2+}, Mn^{2+}, Fe^{3+}, Cu^{2+}, Zn^{2+} and Mg^{2+} (group II) up to 150-fold did not affect the peak current of PAR and DIC oxidation at the ZIF-67/SiO_2NPs/GONs/GCE. Furthermore, a 100-fold excess of biological interferences like ascorbic acid, citric acid, oxalic acid, ciprofloxacin, glucose, sucrose, lactose, starch and urea did not alter the peak current response of PAR or DIC (Fig. S1 in Supporting Information). This study showed that the signal changes in the oxidation peak current of PAR and DIC were less than ± 5%, confirming that the ZIF-67/SiO_2NPs/GONs/GCE exhibits excellent selectivity in the presence of mentioned metal ions and biological molecules.

Stability, repeatability and reproducibility of modified electrode

Stability, repeatability and reproducibility of the present modified electrode was evaluated by DPV method. The stability of the ZIF-67/SiO_2NPs/GONs/GCE was studied for a period of 30 days. The ZIF-67/SiO_2NPs/GONs/GCE was stored in 0.1 M PBS solution (pH = 7.0) at room temperature when not in use. The initial current response for PAR and DIC decreased about 2.4–2.7% and 3.8–4.0% after 5 and 30 days, respectively, indicates good stability of the ZIF-67/SiO_2NPs/GONs/GCE (Fig. S2 A in Supporting Information). The relative standard deviations (RSD) for 7 measurements in a time interval of 1 h of measuring in the concentrations of 30 μM PAR and 60 μM DIC were 3.25% and 3.14%, respectively (Fig. S2 B in Supporting Information). Therefore, the present sensor has good stability and high repeatability. For the testing of the reproducibility of modified electrode, seven ZIF-67/SiO_2NPs/GONs/GCE were fabricated and used independently for PAR (30 μM) and DIC (60 μM) concentrations with RSD of 3.1–3.7%, indicates good reproducibility in the ZIF-67/SiO_2NPs/GONs/GCE preparation process (Fig. S2 C in Supporting Information).

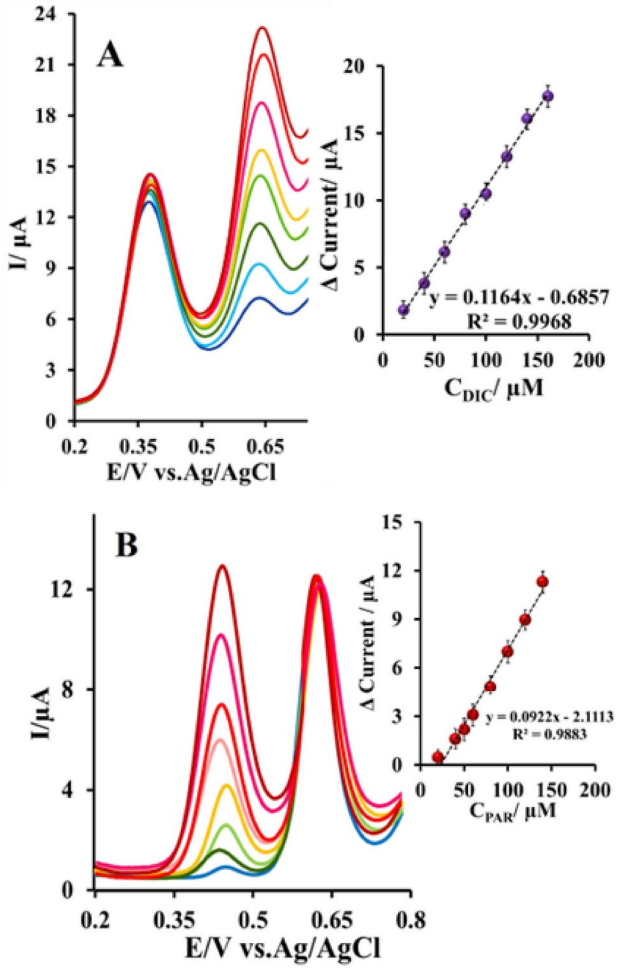

Fig. 12. (**A**) DPV curves for different concentrations of DIC in the presence of a constant concentration of PAR (75 µM) in PBS (0.1 M, pH = 7.0). Inset: calibration curve for DIC in the range of 20–160 µM. (**B**) DPV curves for different concentrations of PAR in the presence of a constant concentration of DIC (50 µM) in PBS (0.1 M, pH = 7.0). Inset: calibration curve for PAR in the range of 20–150 µM.

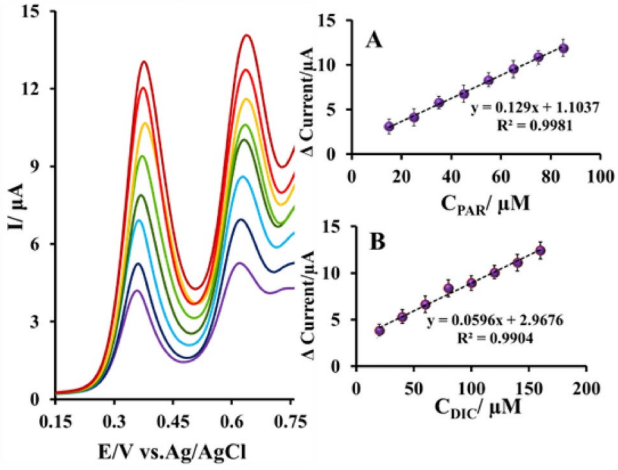

Fig. 13. DPV curves of ZIF-67/SiO_2NPs/GONs/GCE in PBS (0.1 M, pH = 7.0) containing different concentrations of PAR and DIC. [PAR] = 15–85 µM and [DIC] = 20–160 µM. Inset (**A**) calibration plot of ΔIp vs. PAR concentrations and inset (**B**) calibration plot of ΔIp vs. DIC concentrations.

Sample	Declared PAR content	Found content	Recovery (%)	RSD (%)
1	325 (mg/tablet)	331.5	102	2.6
2	325 (mg/tablet)	317.0	97.53	2.9
3	325 (mg/tablet)	321.8	98.8	2.7

Table 3. Determination of PAR in real sample by ZIF-67/SiO_2NPs/GONs/GCE /GCE (n = 3).

Sample	Labeled value (mg)	Found content	Recovery (%)	RSD (%)
1	50 (mg/tablet)	47.98	95.96	3.8
2	50 (mg/tablet)	49.40	98.80	2.8
3	100 (mg/tablet)	96.89	96.89	2.6
4	100 (mg/tablet)	97.65	97.65	3.2

Table 4. Determination of DIC in real sample by ZIF-67/SiO_2NPs/GONs/GCE (n = 3).

Sample	Labeled value (mg)	Found content	Recovery (%)	RSD (%)
DIC& PAR	50 (mg/tablet) DIC &325 PAR (mg/tablet)	46.76 & 316.84	93.52 & 97.48	4.1 & 3.4
DIC & PAR	50 (mg/tablet) DIC & 325 (mg/tablet)PAR	47.70 & 314.57	95.40 & 96.79	3.7 & 3.8

Table 5. Simultaneous determination of PAR and DIC in real sample by ZIF-67/SiO_2NPs/GONs/GCE (n = 3).

Real samples analysis

The concentration of PAR in the real tablet samples (Shafa Pharmaceutical Company, Tehran, Iran) was determined using ZIF-67/SiO_2NPs/GONs/GCE. Firstly, 10 tablets of PAR were weighed and then powdered. The powdered sample was dissolved in 125 mL of double distilled water. Then it was centrifuged at 8000 rpm for 10 min and 5 mL of supernatant was diluted 50 times with PBS (see the preparation of real samples in Supporting Information) and the obtained solution was used as a sample to detect PAR. The standard addition method was used to compare the results of added PAR values. The obtained results are given in Table 3. The RSD% for five parallel determinations for each sample was less than 4%. In addition, the recovery for PAR detection using ZIF-67/SiO_2NPs/GONs/GCE is obtained between 97.53 and 102.0%. The same process on the measurement of DIC in tablet samples (Dana and Iran Najo, Tehran, Iran) has been done and the obtained results are shown in the Table 4. Also, the proposed sensor was used for simultaneous determination of PAR and DIC in the tablets that contain both drugs (DICLOFENAC & PARACETAMOL) (Alphadrug Pharmaceutical Company, India) samples and the obtained results are shown in the Table 5. The reported results in Tables 3, 4 and 5 show that the present sensor; ZIF-67/SiO_2NPs/GONs/GCE, exhibits good performance in the analysis of real pharmaceutical samples containing alone PAR and DIC and also both of them.

Conclusion

As a result, a simple electrochemical sensor was successfully designed and fabricated for rapid, accurate, and selective individual and simultaneous determination of PAR and DIC. The experimental results showed that the ZIF-67/SiO_2NPs/GONs/GCE has excellent electrocatalytic activity toward the PAR and DIC oxidation with obvious increases in the peak currents in compared with bare GCE, GONs/GCE, SiO_2NPs/GONs/GCE and ZIF-67/GCE. The resultant DPV gram exhibited two anodic peaks at 375 (oxidation of PAR) and 640 mV (oxidation of DIC) with a separation of approximately 265 mV. Under optimal conditions, it has been observed that the calibration curves for PAR and DIC exhibit linearity within the concentration ranges of 0.5–190 µM and 0.5–200 µM, with detection limits of 0.29 and 0.132 µM for PAR and DIC, respectively in individual determination. Also, the obtained results showed that the ZIF-67/SiO_2NPs/GONs/GCE sensor is suitable for the simultaneous determination of PAR and DIC with good characteristics such as wide linear range, low detection limit, high stability, and remarkable reproducibility. Based on the above excellent performance, the proposed sensor could be used for efficient determination of PAR and DIC in individual tablets and also both drugs' tablets (DICLOFENAC & PARACETAMOL) samples.

Data availability

All data generated or analysed during this study are included in this published article [and its supplementary information files].

Received: 12 November 2024; Accepted: 12 March 2025
Published online: 19 March 2025

References

1. Jain, R., Jha, R. R., Kumari, A. & Khatri, I. Dispersive liquid–liquid microextraction combined with digital image colorimetry for paracetamol analysis. *Microchem. J.* **162**, 105870 (2021).
2. Freo, U., Ruocco, C., Valerio, A., Scagnol, I. & Nisoli, E. Paracetamol: A review of guideline recommendations. *J. Clin. Med.* **10**(15), 3420 (2021).
3. Silva, H. A descriptive overview of the medical uses given to Mentha aromatic herbs throughout history. *Biology* **9**(12), 484 (2020).
4. Sawan, H. S., Merey, H. A., Mahmoud, A. M. & Atty, S. A. Electrochemical sensor based on ZrO_2/ionic liquid for ultrasensitive simultaneous determination of metoclopramide and paracetamol in biological fluids. *J. Appl. Electrochem.* **54**(3), 703–718 (2024).
5. Purohit, B., Kumar, A., Mahato, K. & Chandra, P. Novel sensing assembly comprising engineered gold dendrites and MWCNT-AuNPs nanohybrid for acetaminophen detection in human urine. *Electroanalysis* **32**(3), 561–570 (2020).
6. Chidiac, A. S., Buckley, N. A., Noghrehchi, F. & Cairns, R. Paracetamol (acetaminophen) overdose and hepatotoxicity: mechanism, treatment, prevention measures, and estimates of burden of disease. *Expert Opinion Drug Metab. Toxicol.* **19**(5), 297–317 (2023).
7. Khan, H. Review on Analytical Methods for Determination of Aceclofenac and Paracetamol. *Asian Journal of Pharmaceutical Analysis* **14**(3), 175–179 (2024).
8. Melo, L. M., Souza, K. A., Lopes, J. E., Muñoz, R. A., Costa, J. L., dos Santos, W. T. Electrochemical methods for the determination of acetaminophen in biological matrices: A critical review for clinical analysis. *Anal. Chim. Acta* (2024) 343243.
9. Bariguian Revel, F., Fayet, M. & Hagen, M. Topical diclofenac, an efficacious treatment for osteoarthritis: A narrative review. *Rheumatol. Ther.* **7**(2), 217–236 (2020).
10. Sparidans, R. W., Lagas, J. S., Schinkel, A. H., Schellens, J. H. & Beijnen, J. H. Liquid chromatography-tandem mass spectrometric assay for diclofenac and three primary metabolites in mouse plasma. *J. Chromatogr. B* **872**(1–2), 77–82 (2008).
11. Alfaro, R. A., Davis, D. D., Diclofenac. [Updated 2023 May 22]. In: StatPearls [Internet]. Treasure Island (FL): StatPearls Publishing; 2025 Jan-. Available from: https://www.ncbi.nlm.nih.gov/books/NBK557879/.
12. Kevin, O. O., Yan, K., Feng, J. & Zhang, J. Label-free photoelectrochemical aptasensing of diclofenac based on gold nanoparticles and graphene-doped CdS. *Sens. Actuators B: Chem.* **256**, 334–341 (2018).
13. Honakeri, N. C., Malode, S. J., Kulkarni, R. M. & Shetti, N. P. Electrochemical behavior of diclofenac sodium at coreshell nanostructure modified electrode and its analysis in human urine and pharmaceutical samples. *Sens. Int.* **1**, 100002 (2020).
14. Gouda, A. A., El-Sayed, M. I. K., Amin, A. S. & El Sheikh, R. Spectrophotometric and spectrofluorometric methods for the determination of non-steroidal anti-inflammatory drugs: A review. *Arab. J. Chem.* **6**(2), 145–163 (2013).
15. Mini, S. U. Chromatographic methods for the determination of diclofenac in human biological samples: A mini review. *Malays. J. Anal. Sci.* **27**(3), 563–572 (2023).
16. Kassahun, G. S., Griveau, S., Bedioui, F. & Slim, C. Input of electroanalytical methods for the determination of diclofenac: A review of recent trends and developments. *ChemElectroChem* **9**(2), 202100734 (2022).
17. Aguilar-Lira, G. Y. et al. Artificial neural network for the voltamperometric quantification of diclofenac in presence of other nonsteroidal anti-inflammatory drugs and some commercial excipients. *J. Electroanal. Chem.* **801**, 527–535 (2017).
18. Gago-Ferrero, P., Borova, V., Dasenaki, M. E. & Thomaidis, NS. Simultaneous determination of 148 pharmaceuticals and illicit drugs in sewage sludge based on ultrasound-assisted extraction and liquid chromatography-tandem mass spectrometry. *Anal. Bioanal. Chem.* **407**, 4287–4297 (2015).
19. Baghel, S. & Shah, K. A review on methods developed for estimation of paracetamol in combination with other drugs. *Int. J. Pharm. Res. Allied Sci.* **12**, 75–94 (2023).
20. Azish, N., Pourbasheer, E., Imanzadeh, H. & Amiri, M. A chemometric-assisted voltammetric method for simultaneous determination of acetaminophen and diclofenac. *ChemistrySelect* **9**(16), e202305023 (2024).
21. Sasal, A., Tyszczuk-Rotko, K., Wójciak, M., Sowa, I. & Kuryło, M. Simultaneous analysis of paracetamol and diclofenac using MWCNTs-COOH modified screen-printed carbon electrode and pulsed potential accumulation. *Materials* **13**(14), 3091 (2020).
22. Kozak, J., Tyszczuk-Rotko, K., Wójciak, M. & Sowa, I. Electrochemically activated screen-printed carbon sensor modified with anionic surfactant (aSPCE/SDS) for simultaneous determination of paracetamol, diclofenac and tramadol. *Materials* **14**(13), 3581 (2021).
23. Kokab, T. et al. Simultaneous femtomolar detection of paracetamol, diclofenac, and orphenadrine using a carbon nanotube/zinc oxide nanoparticle-based electrochemical sensor. *ACS Appl. Nano Mater.* **4**(5), 4699–4712 (2021).
24. Cetinkaya, A., Kaya, S. I., Ozcelikay, G., Budak, F. & Ozkan, S. A. Carbon nanomaterials-based novel hybrid platforms for electrochemical sensor applications in drug analysis. *Crit. Rev. Anal. Chem.* **54**(5), 1227–1242 (2024).
25. Vernekar, P. R., Purohit, B., Shetti, N. P. & Chandra, P. Glucose modified carbon paste sensor in the presence of cationic surfactant for mefenamic acid detection in urine and pharmaceutical samples. *Microchem. J.* **160**, 105599 (2021).
26. Azad, U. P., Chandra, P. *Handbook of Nanobioelectrochemistry*, Springer, 1 (2023).
27. Baranwal, A., Chiranjivi, A. K., Kumar, A., Dubey, V. K. & Chandra, P. Design of commercially comparable nanotherapeutic agent against human disease-causing parasite, Leishmania. *Sci. Rep.* **8**(1), 8814 (2018).
28. Demir, E., Ozdogan, N. A., Olcer, M. Nanostructured electrochemical biosensors for estimation of pharmaceutical drugs. *Novel Nanostruct. Mater. Electrochem. Bio-Sensing Appl*. Elsevier 2024, pp. 379–428.
29. Purohit, B., Kumar, A., Mahato, K., Roy, S., Chandra, P. Cancer cytosensing approaches in miniaturized settings based on advanced nanomaterials and biosensors, In *Nanotechnology in Modern Animal Biotechnology*, (2019) (133–147), Elsevier.
30. Wadhwa, R. et al. Red blood cells as an efficient in vitro model for evaluating the efficacy of metallic nanoparticles. *3 Biotech* **9**, 1–15 (2019).
31. Kumar, A. et al. Gold-iron bimetallic nanoparticles impregnated reduced graphene oxide based nanosensor for label-free detection of biomarker related to non-alcoholic fatty liver disease. *Electroanalysis* **31**(12), 2417–2428 (2019).
32. Liu, D., Yuan, B. *Preparation of Nanomaterial Modified Electrode and Its Sensing Application*. MDPI-Multidisciplinary Digital Publishing Institute 2022.
33. Shanbhag, M. M., Bukkitgar, S. D., Sharma, P. & Shetti, N. P. *Nanostructured Electrodes* 147–175 (Elsevier, 2022).
34. Tonelli, D., Gualandi, I., Musella, E. & Scavetta, E. Synthesis and characterization of layered double hydroxides as materials for electrocatalytic applications. *Nanomaterials* **11**(3), 725 (2021).
35. Wu, X. et al. Application of MXene in electrochemical sensors: A review. *Electroanalysis* **33**(8), 1827–1851 (2021).
36. Chuang, C. H. & Kung, C. W. Metal-organic frameworks toward electrochemical sensors: Challenges and opportunities. *Electroanalysis* **32**(9), 1885–1895 (2020).
37. Habibi, B., Pashazadeh, A. & Pashazadeh, S. Improving the electrocatalytic activity of the copper (II) metal-organic framework by functionalized imidazolate linker and functionalized carbon nanoparticles for detection of acyclovir. *J. Electroanal. Chem.* **971**, 118595 (2024).
38. Makani, S., Habibi, B. & Mohammad-Rezaei, R. Fabrication of a fast response non-enzymatic glucose sensor based on in-situ synthesized Cu-metal organic frameworks integrated with electrochemically reduced graphene quantum dots. *Nanomed. J.* **12**(1), 18–32 (2025).
39. Ma, M. et al. Synthesis, structure and electrochemical properties of Co-MOF containing pyridine polycarboxylic acid. *J. Solid State Chem.* **333**, 124648 (2024).
40. Kalimuthu, P., Ramachandran, R., Anushya, G. Metal-Organic Framework for Electrochemical Biosensing Applications, Handbook of Nanobioelectrochemistry: Application in Devices and Biomolecular Sensing, Springer, 2023, 661–686.

41. Rezapour, K., Habibi, B. & Imanzadeh, H. New type nanocomposite based on metal-organic frameworks decorated with nickel nanoparticles as a potent electrocatalyst for methanol oxidation in alkaline media. *Int. J. Hydrog. Energy* **69**, 518–531 (2024).
42. Mousavi, S. M. et al. Recent advances and synergistic effect of bioactive zeolite imidazolate frameworks (ZIFs) for biosensing applications. *Talanta* **275**, 126097 (2024).
43. Habibi, B., Pashazadeh, A., Pashazadeh, S. & Saghatforoush, L. A. Copper/zeolitic imidazolate framework-8 integrated by boron nitride as an electrocatalyst at the glassy carbon electrode to sensing of the clopidogrel. *J. Solid State Chem.* **323**, 123982 (2023).
44. Cheng, N., Ren, L., Xu, X., Du, Y. & Dou, S. X. Recent development of zeolitic imidazolate frameworks (ZIFs) derived porous carbon based materials as electrocatalysts. *Adv. Energy Mater.* **8**(25), 1801257 (2018).
45. Vinodh, R. et al. Recent advancements of polyaniline/metal organic framework (PANI/MOF) composite electrodes for supercapacitor applications: A critical review. *Nanomaterials* **12**(9), 1511 (2022).
46. Sadegh, N., Dehcheshmeh, I. M., Sadegh, F. Review of zeolitic imidazolate framework/graphene oxide: a synergy of synthesis, properties and function for multifaceted applications in nanotechnology. *FlatChem*, (2024) 100618.
47. Chafiq, M., Chaouiki, A., Al-Moubaraki, A. H., Ko, Y. G. Recent progress in ZIF nanocomposite materials for wastewater pollutant in aqueous solution: A mini-review. *Process Safety Environ. Prot.* (2024).
48. Shumba, M., Centane, S., Chindeka, F. & Nyokong, T. Nanocomposites of sulphur-nitrogen co-doped graphene oxide nanosheets and cobalt mono carboxyphenoxy phthalocyanines for facile electrocatalysis. *J. Electroanal. Chem.* **791**, 36–48 (2017).
49. Aftab, K., Riaz, A. *Graphene-based electrochemical sensors*. *Nanomaterials-Based Electrochemical Sensors: Properties, Applications and Recent Advances*, Elsevier 2024, pp. 269–293.
50. Li, J. et al. Polyaniline composited with rGO wrapped-SiO_2 microsphere ammonia sensor with fast response/recovery and high sensitivity for pig healthy breeding. *Sens. Actuators B Chem.* **398**, 134784 (2024).
51. Zhao, H. et al. Fabrication of gallic acid electrochemical sensor based on interconnected Super-P carbon black@mesoporous silica nanocomposite modified glassy carbon electrode. *J. Market Res.* **24**, 2100–2112 (2023).
52. Zhao, H. et al. Facile synthesis of silicon dioxide nanoparticles decorated multi-walled carbon nanotubes with graphitization and carboxylation for electrochemical detection of gallic acid. *Ceram. Int.* **49**, 26289–26301 (2023).
53. Li, M., Chen, C., Chen, Z., Shen, K. & Yang, L. Structural design and antibacterial properties of porous SiO_2NPs/ZnO/Cu_2O composites. *Mater. Express* **14**(4), 572–582 (2024).
54. Zhang, C. et al. Study on structural and functional properties of porous SiO_2NPs core-shell construction/polyethylene nanocomposites with enhanced interfacial interaction. *J. Appl. Polym. Sci.* **139**(19), 52115 (2022).
55. Rani, P., Kasneryk, V. & Opanasenko, M. MOF-inorganic nanocomposites: Bridging a gap with inorganic materials. *Appl. Mater. Today* **26**, 101283 (2022).
56. Wang, Y., Zhu, S., Guan, H. & Man, Q. Silica coated MOFs-derived composites with excellent electromagnetic wave absorption and corrosion resistance. *Colloids Surf. A: Physicochem. Eng. Aspects* **694**, 134043 (2024).
57. Derbe, T., Sani, T., Amare, E. & Girma, T. Mini review on synthesis, characterization, and application of zeolite@MOF composite. *Adv. Mater. Sci. Eng.* **2023**(1), 8760967 (2023).
58. An, J. et al. Structure and properties of epoxy resin/graphene oxide composites prepared from silicon dioxide-modified graphene oxide. *ACS Omega* **9**(15), 17577–17591 (2024).
59. Hao, Q. et al. Preparation of GO-SiO_2 NPs three-dimensional point-plane nanomaterials and enhancement of epoxy resin mechanical property. *Polym. Compos.* **45**(2), 1266–1277 (2024).
60. Lan, X. et al. Preparation of SiO_2 NPs/rGO/CNTs composite and application for lithium-ion-battery anodes. *Mater. Lett.* **353**, 135300 (2023).
61. Kheirkhah, R., Badoei-dalfard, A., Karami, Z. Encapsulation and biochemical characterization of Lipase on a silica-coated@ZIF-8@/graphene oxide (GSLZIF) and its application on the biodiesel production. *J. Iran. Chem. Soc.* (2021) 1–13.
62. Muslihati, A., Gumilar, G., Nugraha, N., Wasisto, H. S., Yuliarto, B. Synthesis and characterization of ZIF 67 manganese bimetal for electrochemical sensor application. *J. Phys.: Conf. Ser.* IOP Publishing, (2024) 012007.
63. Pendashteh, A., Mousavi, M. F. & Rahmanifar, M. S. Fabrication of anchored copper oxide nanoparticles on graphene oxide nanosheets via an electrostatic coprecipitation and its application as supercapacitor. *Electrochim. Acta* **88**, 347–357 (2013).
64. Swetha, N., Venkata-Lakshmi, V., Mylarappa, M., Chandruvasan, S. & Harisha, K. S. Development of SiO_2NPs/rGO from rice husk for photocatalysis, antioxidant, electrochemical and green sensor detection studies. *Silicon* **16**(9), 4037–4059 (2024).
65. Habibi, B. & Pashazadeh, S. Fabrication, characterization and performance evaluation of an amplified electrochemical sensor based on MOFs nanocomposite for leukemia drug Imatinib determination. *Sens. Bio-Sens. Res.* **42**, 100604 (2023).
66. Hu, Y. et al. Advances in electrochemical sensing with ZIF-67 and related materials. *Int. J. Electrochem. Sci.* **18**(7), 100180 (2023).
67. Wulandari, C., Gumilar, G., Wasisto, H., Iqbal, M., Nugroho, W., Rusydi, F. Preparation and properties of bimetallic Co/Cu ZIF-67 for electrochemical application. *J. Phys.: Conf. Ser.*, IOP Publishing, (2024) 012004.
68. Siburian, R., Sihotang, H., Raja, S. L., Supeno, M. & Simanjuntak, C. New route to synthesize of graphene nano sheets. *Orient. J. Chem.* **34**(1), 182 (2018).
69. Liu, L., Guo, X., Shi, L., Chen, L., Zhang, F., Li, A. SiO_2-GO nanofillers enhance the corrosion resistance of waterborne polyurethane acrylic coatings. *Adv. Compos. Lett.* **29**, 2633366X20941524 (2020).
70. Al-Murisi, M. et al. In situ growth of zeolite imidazole frameworks (ZIF-67) on carbon cloth for the application of oxygen reduction reactions and microbial fuel cells. *ACS Omega* **8**(47), 44514–44522 (2023).
71. Habibi, B., Pashazadeh, S., Saghatforoush, L. A. & Pashazadeh, A. A thioridazine hydrochloride electrochemical sensor based on zeolitic imidazolate framework-67-functionalized bio-mobile crystalline material-41 carbon quantum dots. *N. J. Chem.* **45**(32), 14739–14750 (2021).
72. Habibi, B. & Pashazadeh, S. Design and fabrication of a novel platform for detection of 5-fluorouracil as the anti-cancer drug using COFs/MOFs nanocomposite with graphene quantum dots. *Microchem. J.* **207**, 111657 (2024).
73. Hajmalek, S., Jahani, S. & Foroughi, M. M. Simultaneous voltammetric determination of tramadol and paracetamol exploiting glassy carbon electrode modified with $FeNi_3$ nanoalloy in biological and pharmaceutical media. *ChemistrySelect* **6**(33), 8797–8808 (2021).
74. Shafiei, H., Haqgu, M., Nematollahi, D. & Gholami, M. R. An experimental and computational study on the rate constant of electrochemically generated N-acetyl-p-quinoneimine with dimethylamine. *Int. J. Electrochem. Sci.* **3**(10), 1092–1107 (2008).
75. Stefano, J. S., Montes, R. H., Richter, E. M. & Muñoz, R. A. Flow-injection analysis with multiple-pulse amperometry for simultaneous determination of paracetamol and naproxen using a homemade flow cell for screen-printed electrodes. *J. Braz. Chem. Soc.* **25**, 484–491 (2014).
76. Makhoul, E. et al. Cobalt-substituted porous calcium copper titanate electrodes for paracetamol degradation by an electro-oxidation/peroxymonosulfate system. *Appl. Surf. Sci.* **669**, 160430 (2024).
77. Porada, R. et al. Targeted modification of the carbon paste electrode by natural zeolite and graphene oxide for the enhanced analysis of paracetamol. *Microchem. J.* **187**, 108455 (2023).
78. Leve, Z. D., Jahed, N., Sanga, N. A., Iwuoha, E. I. & Pokpas, K. Determination of paracetamol on electrochemically reduced graphene oxide-antimony nanocomposite modified pencil graphite electrode using adsorptive stripping differential pulse voltammetry. *Sensors* **22**(15), 5784 (2022).
79. Xia, Y. et al. Energy-efficient electrochemical treatment of paracetamol using a PbO_2 anode based on pulse electrodeposition strategy: Kinetics, energy consumption and mechanism. *Environ. Res.* **216**, 114673 (2023).

80. Cid-Cerón, M. M. et al. New insigths on the kinetics and mechanism of the electrochemical oxidation of diclofenac in neutral aqueous medium. *Electrochim. Acta* **199**, 92–98 (2016).
81. Nasiri, F., Rounaghi, G. H., Ashraf, N. & Deiminiat, B. A new electrochemical sensing platform for quantitative determination of diclofenac based on gold nanoparticles decorated multiwalled carbon nanotubes/graphene oxide nanocomposite film. *Int. J. Environ. Anal. Chem.* **101**(2), 153–166 (2021).
82. Mirceski, V., Guziejewski, D. & Gulaboski, R. Genuine anodic and cathodic current components in cyclic voltammetry. *Sci. Rep.* **14**(1), 17314 (2024).
83. Come, J., Taberna, P. L., Hamelet, S., Masquelier, C. & Simon, P. Electrochemical kinetic study of $LiFePO_4$ using cavity microelectrode. *J. Electrochem. Soc.* **158**(10), A1090 (2011).
84. Deehan, L., Kaushik, A. K., Chaudhary, G. R., Papakonstantinou, P. & Bhalla, N. Decoupling variable capacitance and diffusive components of active solid-liquid interfaces with flex points. *ACS Meas. Sci. Au* **4**(5), 599–605 (2024).
85. Habibi, B., Pashazadeh, S., Saghatforoush, L. A. & Pashazadeh, A. Direct electrochemical synthesis of the copper based metal-organic framework on/in the heteroatoms doped graphene/pencil graphite electrode: Highly sensitive and selective electrochemical sensor for sertraline hydrochloride. *J. Electroanal. Chem.* **888**, 115210 (2021).
86. Ejaz, A. & Jeon, S. A highly stable and sensitive GO-XDA-Mn_2O_3 electrochemical sensor for simultaneous electrooxidation of paracetamol and ascorbic acid. *Electrochimica Acta* **245**, 742–751 (2017).
87. Zhang, Y. et al. ZIF-67-derived highly dispersed Co_3O_4 nanoparticles@hollow carbon chamfer cube-reduced graphene oxide for electrochemical detection of dopamine, acetaminophen and xanthine. *J. Alloys Compd.* **936**, 168155 (2023).
88. Huang, Y. et al. Preparation of carbon fiber composite modified by cobalt lanthanum oxides and its electrochemical simultaneous determination of amlodipine and acetaminophen. *Adv. Fiber Mater.* **4**(5), 1153–1163 (2022).
89. Yang, H. et al. Nitrogen-doped carbon@TiO_2 double-shelled hollow spheres as an electrochemical sensor for simultaneous determination of dopamine and paracetamol in human serum and saliva. *J. Pharm. Anal.* **12**(3), 436–445 (2022).
90. Anh, N. T., Van Quy, N., Van Hoang, O., Dinh, N. X. & Le, A.-T. An on-site and portable electrochemical sensing platform based on spinel zinc ferrite nanoparticles for the quality control of paracetamol in pharmaceutical samples. *Nanoscale Adv.* **6**(1), 256–267 (2024).
91. Barsan, M. M., Toledo, C. T. & Brett, C. M. New electrode architectures based on poly (methylene green) and functionalized carbon nanotubes: Characterization and application to detection of acetaminophen and pyridoxine. *J. Electroanal. Chem.* **736**, 8–15 (2015).
92. Charithra, M. M. & Manjunatha, J. G. Enhanced voltammetric detection of paracetamol by using carbon nanotube modified electrode as an electrochemical sensor. *J. Electrochem. Sci. Eng.* **10**(1), 29–40 (2020).
93. Teglia, C. M., Gutierrez, F. A. & Goicoechea, H. C. Natural deep eutectic solvent: A novelty alternative as multi-walled carbon nanotubes dispersing agent for the determination of paracetamol in urine. *Talanta* **242**, 123290 (2022).
94. Filik, H., Çetintaş, G., Avan, A. A., Koç, S. N. & Boz, İ. Electrochemical sensing of acetaminophen on electrochemically reduced graphene oxide-nafion composite film modified electrode. *Int. J. Electrochem. Sci.* **8**(4), 5724–5737 (2013).
95. Magerusan, L., Pogacean, F. & Pruneanu, S. Enhanced acetaminophen electrochemical sensing based on nitrogen-doped graphene. *Int. J. Mol. Sci.* **23**(23), 14866 (2022).
96. Krampa, F. D., Aniweh, Y., Kanyong, P. & Awandare, G. A. Graphene nanoplatelet-based sensor for the detection of dopamine and N-acetyl-p-aminophenol in urine. *Arab. J. Chem.* **13**(1), 3218–3225 (2020).
97. Liang, W. et al. Nitrogen-rich porous carbon modified electrochemical sensor for the detection of acetaminophen. *J. Electroanal. Chem.* **855**, 113496 (2019).
98. Zhao, P. et al. Stimuli-enabled switch-like paracetamol electrochemical sensor based on thermosensitive polymer and MWCNTs-GQDs composite nanomaterial. *Nanoscale* **11**(15), 7394–7403 (2019).
99. Chen, X., Zhu, J., Xi, Q. & Yang, W. A high performance electrochemical sensor for acetaminophen based on single-walled carbon nanotube–graphene nanosheet hybrid films. *Sens. Actuators B: Chem.* **161**(1), 648–654 (2012).
100. Prasad, G. V., Vinothkumar, V., Jang, S. J. & Kim, T. H. Multi-walled carbon nanotube/graphene oxide/poly (threonine) composite electrode for boosting electrochemical detection of paracetamol in biological samples. *Microch. J.* **184**, 108205 (2023).
101. Ma, B. et al. Electrocatalysis of Cu–MOF/graphene composite and its sensing application for electrochemical simultaneous determination of dopamine and paracetamol. *Electroanalysis* **31**(6), 1002–1008 (2019).
102. Shih, Y. J., Wu, Z. L. & Lin, S. K. Electrochemical detection of paracetamol using zeolitic imidazolate framework and graphene oxide derived zinc/nitrogen-doped carbon. *Sens. Actuators B: Chem.* **409**, 135600 (2024).
103. Baccarin, M. et al. Electrochemical sensor based on reduced graphene oxide/carbon black/chitosan composite for the simultaneous determination of dopamine and paracetamol concentrations in urine samples. *J. Electroanal. Chem.* **799**, 436–443 (2017).
104. Houshmand, M., Jabbari, A., Heli, H., Hajjizadeh, M. & Moosavi-Movahedi, A. Electrocatalytic oxidation of aspirin and acetaminophen on a cobalt hydroxide nanoparticles modified glassy carbon electrode. *J. Solid State Electrochem.* **12**, 1117–1128 (2008).
105. Hefnawy, M. A., Medany, S. S., Fadlallah, S. A., El-Sherif, R. M. & Hassan, S. S. Novel self-assembly Pd (II)-schiff base complex modified glassy carbon electrode for electrochemical detection of paracetamol. *Electrocatalysis* **13**(5), 598–610 (2022).
106. Rajamani, A. R. & Peter, S. C. Novel nanostructured Pt/CeO_2@Cu_2O carbon-based electrode to magnify the electrochemical detection of the neurotransmitter dopamine and analgesic paracetamol. *ACS Appl. Nano Mater.* **1**(9), 5148–5157 (2018).
107. Ismail, K. M., Hassan, S. S., Medany, S. S. & Hefnawy, M. A. A facile sonochemical synthesis of the Zn-based metal-organic framework for electrochemical sensing of paracetamol. *Mater. Adv.* **5**(14), 5870–5884 (2024).
108. Ranjitha, N. et al. Synthesis, characterization, biological applications of novel coumarine azo-dye ligand and its transition metal complexes: Simultaneous electrochemical detection of paracetamol and uric acid. *Polyhedron* **253**, 116909 (2024).
109. Eteya, M. M., Rounaghi, G. H. & Deiminiat, B. Fabrication of a new electrochemical sensorbased on AuPt bimetallic nanoparticles decorated multi-walled carbon nanotubes for determination of diclofenac. *Microchem. J.* **144**, 254–260 (2019).
110. Franco-Guzmán, M., Mendoza-Huizar, L. H., Roa-Morales, G., Galán-Vidal, C. A. & Álvarez-Romero, G. A. Voltammetric quantification of diclofenac using a modified CPE enriched with TiO_2 nanoparticles and MWCNT. *J. Electrochem. Soc.* **168**(3), 037502 (2021).
111. Ensafi, A. A., Izadi, M. & Karimi-Maleh, H. Sensitive voltammetric determination of diclofenac using room-temperature ionic liquid-modified carbon nanotubes paste electrode. *Ionics* **19**, 137–144 (2013).
112. Chethana, B. K., Basavanna, S. & Arthoba-Naik, Y. Voltammetric determination of diclofenac sodium using tyrosine-modified carbon paste electrode. *Ind. Eng. Chem. Res.* **51**(31), 10287–10295 (2012).
113. Zhang, C. et al. An electrochemical sensor based on plasma-treated zinc oxide nanoflowers for the simultaneous detection of dopamine and diclofenac sodium. *Microchem. J.* **158**, 105237 (2020).
114. Singh, A. K., Gautam, R. K., Agrahari, S. & Tiwari, I. Oxidized g-C_3N_4 decorated with Cu-Al layered double hydroxide as a sustainable electrochemical sensing material for quantification of diclofenac. *Mater. Chem. Phys.* **294**, 127002 (2023).
115. Mokhtari, A., Karimi-Maleh, H., Ensafi, A. A. & Beitollahi, H. Application of modified multiwall carbon nanotubes paste electrode for simultaneous voltammetric determination of morphine and diclofenac in biological and pharmaceutical samples. *Sens. Actuators B: Chem.* **169**, 96–105 (2012).
116. Slim, C., Tlili, N., Richard, C., Griveau, S. & Bedioui, F. Amperometric detection of diclofenac at a nano-structured multi-wall carbon nanotubes sensing films. *Inorgan. Chem. Commun.* **107**, 107454 (2019).

117. Mostafavi, M., Yaftian, M. R., Piri, F. & Shayani-Jam, H. A new diclofenac molecularly imprinted electrochemical sensor based upon a polyaniline/reduced graphene oxide nano-composite. *Biosens. Bioelectron.* **122**, 160–167 (2018).
118. Hajjizadeh, M., Jabbari, A., Heli, H., Moosavi-Movahedi, A. A. & Haghgoo, S. Electrocatalytic oxidation of some anti-inflammatory drugs on a nickel hydroxide-modified nickel electrode. *Electrochim. Acta* **53**(4), 1766–1774 (2007).
119. Kashefi-Kheyrabadi, L. & Mehrgardi, M. A. Design and construction of a label free aptasensor for electrochemical detection of sodium diclofenac. *Biosens. Bioelectron.* **33**(1), 184–189 (2012).
120. Gimenes, D. T., De Freitas, J. M., Munoz, R. A. A. & Richter, E. M. Flow-injection amperometric method for determination of diclofenac in pharmaceutical formulations using a boron-doped diamond electrode. *Electroanalysis* **23**(11), 2521–2525 (2011).
121. Aguilar-Lira, G. Y. et al. New insights on diclofenac electrochemistry using graphite as working electrode. *J. Electroanal. Chem.* **794**, 182–188 (2017).
122. Shamsipur, M., Jalali, F. & Ershad, S. Preparation of a diclofenac potentiometric sensor and its application to pharmaceutical analysis and to drug recovery from biological fluids. *J. Pharm. Biomed. Anal.* **37**(5), 943–947 (2005).
123. Rodríguez, J. A., Barrado, E., Castrillejo, Y., Santos, J. R. & Lima, J. L. F. C. Validation of a tubular bismuth film amperometric detector: Determination of diclofenac sodium by multisyringe flow injection analysis. *J. Pharm. Biomed. Anal.* **45**(1), 47–53 (2007).
124. Ambrosi, A., Antiochia, R., Campanella, L., Dragone, R. & Lavagnini, I. Electrochemical determination of pharmaceuticals in spiked water samples. *J. Hazard. Mater.* **122**(3), 219–225 (2005).
125. Bahadori, Y. & Razmi, H. Design of an electrochemical platform for the determination of diclofenac sodium utilizing a graphenized pencil graphite electrode modified with a Cu–Al layered double hydroxide/chicken feet yellow membrane. *N. J. Chem.* **45**(32), 14616–14625 (2021).

Acknowledgements

The authors gratefully acknowledge the Research Council of Azarbaijan Shahid Madani University for its financial support. Also, the authors sincerely thank the Central Laboratory of Azarbaijan Shahid Madani University for conducting the SEM and EDX experiments (Phenom ProX Desktop SEM) as part of this study.

Author contributions

Biuck Habibi: Supervision, Monitoring, Editing, Discussing and Revising. Younes Bahadori: some of the practical works in lab, Visualization, Investigation, Writing- Reviewing and Editing and Data curation. Sara Pashazadeh: some of the practical works in lab, Visualization, Investigation, Writing- Reviewing and Editing and Data curation. Ali Pashazadeh: some of the practical works in lab, Visualization, Investigation, Writing- Reviewing and Editing and Data curation.

Declarations

Competing interests

The authors declare no competing interests.

Additional information

Supplementary Information The online version contains supplementary material available at https://doi.org/10.1038/s41598-025-94178-9.

Correspondence and requests for materials should be addressed to B.H. or Y.B.

Reprints and permissions information is available at www.nature.com/reprints.

Publisher's note Springer Nature remains neutral with regard to jurisdictional claims in published maps and institutional affiliations.